2011

Investigation of the structural behavior of historical covered timber bridges

Allison Machtemes
Iowa State University

Investigation of the structural behavior of historical covered timber bridges

by

Allison Ann Machtemes

A thesis submitted to the graduate faculty
in partial fulfillment of the requirements for the degree of
MASTER OF SCIENCE

Major: Civil Engineering (Structural Engineering)
Program of Study Committee:

Fouad Fanous, Major Professor
Terry Wipf
Vinay Dayal

Iowa State University
Ames, Iowa
2011

DEDICATION

I would like to thank my parents, Pat and Kathy Machtemes, for their continual support, encouragement and direction throughout my entire education. Thank you for realizing my potential, allowing me to develop into the person I am, providing me the opportunities of a lifetime and always pushing me to strive for the best.

Also, to my sister, Abbey, thank you for always standing by me and being my little sister. I really have appreciated your presence during this time and will carious the time we have had together at Iowa State.

Lastly, without the support and continuous encouragement from my future husband, Jordan, I would not have been able to complete this work.

TABLE OF CONTENTS

LIST OF FIGURES

LIST OF TABLES

ACKNOWLEDGEMENTS

The study for this thesis was conducted by the author as part of the ongoing research project entitled *Improved Analytical Techniques for Historic Covered Bridges* (Project No. 10-JV-11111133-016), which is funded through a cooperative research program for covered bridges by the Federal Highway Administration (FHWA) and Forest Products Laboratory (FPL).

The author would not have been able to complete this study without the guidance and assistance from her major professor, Dr. Fouad Fanous. She appreciates all the time and energy that he has put forth to complete this study.

For their continuing support, the author would like to acknowledge Dr. Terry Wipf and Travis Hosteng for their knowledge in the areas related to timber and timber bridges. Also, the author would like to extend her appreciation to James Wacker and Douglas Rammer from FPL for their assistance through the entire project.

Also, the author appreciates the assistance from Kevin Loiselle from Clark Dietz in supplying as built plan sheets, inspection reports of the bridges and for conversations related to the rehabilitation of the Zacke Cox Bridge. The study would not have been completed without the assistance from the Parke County Public Works by providing the load trucks for field testing.

And finally, the author would like to extend her appreciation to Douglas Wood and Owen Steffen for their assistance in conducting the collection of the field data for each of the bridges tested in Indiana.

ABSTRACT

Due to the importance of historical timber covered bridges throughout history, their preservation is necessary. However, conducting an accurate structural evaluation of these types of bridges has always caused difficulties to engineers. Little laboratory and analytical modeling has been previously completed to evaluate the overall behavior and rating of these structures. Within this study, field testing results of displacements and strains for three Burr arch covered timber bridges were completed. Analysis of one of the two main supporting elements, i.e. the truss-arch elements, of the bridge structure was performed using the finite element method which included the as built geometry, such as the splice joints, in the top and bottom chord truss members. The connectivity between timber members, i.e., the connection between vertical and diagonal members, was also accounted for within the model. Finite element analyses included the evaluation of both two and three dimensional stick modeling to evaluate the effect of different modeling techniques that may be utilized by bridge engineers in the evaluation of the structural behavior of these bridges. Through this evaluation, recommendations were developed for the most appropriate analytical finite element model to analyze historical timber covered bridges.

CHAPTER 1: INTRODUCTION

1.1 Background

Before bridges were built, in many locations there were ferries which were used to cross rivers. Due to the necessity of transporting goods, services, and people across the water, ferries were known for having a monopoly over the local economy due to the prices they charged to cross the river. Thus for a business owner that operated on one side of the bank but did business with a buyer on the other side of the bank, they would need to pay the ferry to visit his buyer. With this added cost to transport goods, the public urged their local governments to build bridges. (History of Covered Bridges (2010)). Also, expansion across the United States countryside caused the need for bridges to be built to allow access for personal travel and transportation of goods. During the 19th century, the economic material to build bridges was timber due to its abundant availability, cost, and ease of construction. With the need for bridges to cross obstacles, patents began to be issued for truss designs. Many of the well-known patents included those submitted by Theodore Burr (Burr arch), Ithiel Town (Town lattice), Stephen Long (Long truss), and William Howe (Howe truss). (US Department of Transportation Federal Highway Administration (2005)). In the hopes of building more structures, over time, it was noticed that the joints and wood would deteriorate rather quickly due to the exposure to elements such as water, sun, snow and ice. To protect the wood bridges from these elements, they were covered to extend the life of the structure. Due to the availability of timber and the need for a safe way to cross the lands, thousands of wood covered bridges were built during the 19th and early 20th centuries with many different types of configurations. (History of Covered Bridges (2010)).

With the industry boom during the 19th century and the popularity of the automobile increasing, the use of iron and steel in the construction of bridges became increasingly popular. But during the steel crisis of World War I, timber bridges became popular again. Over time, the use of timber bridges has become non-existent due to the cost, maintenance, and structural capacity of the material over steel fabrication. The uncertainty and evaluation of the timber bridges' structural capacity was noticed through the development of multiple configurations of the truss. From the basic kingpost truss to the burr arch truss that expanded the concepts of the kingpost and added additional strength through the addition of an arch,

from the Warren, Howe and Pratt trusses. (History of Covered Bridges (2010)). With the decline in the use of wood as a material to build bridges, these types of bridges have become distinct historical landmarks which require restoration to preserve the rich history behind these bridge structures. As can be seen in the following figures (Figure 1.1 to 1.7) from the Federal Highway Administration (FHWA) Covered Bridge Manual, each type of bridge has many of the same characteristics but each is uniquely different enough to cause concern when evaluating the structural behavior of each bridge. Below in Table 1.1 is a list of the current number of surviving bridge types.

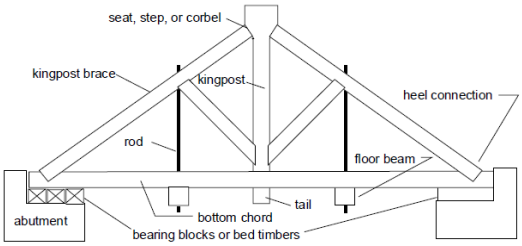

Figure 1.1: Kingpost truss

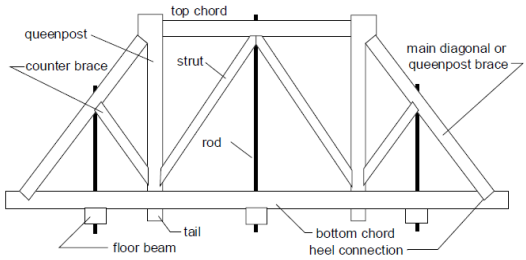

Figure 1.2: Queenpost truss

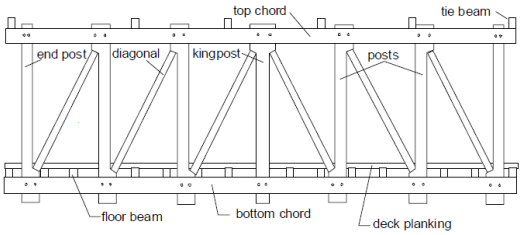

Figure 1.3: Multiple kingpost truss

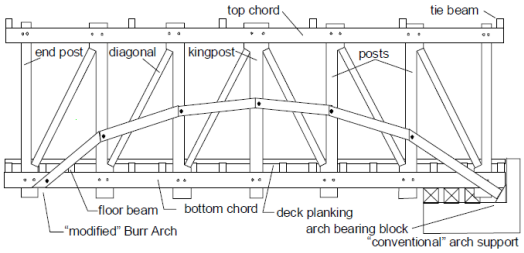

Figure 1.4: Burr arch truss

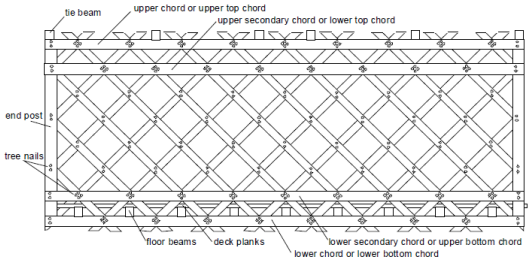

Figure 1.5: Town lattice truss

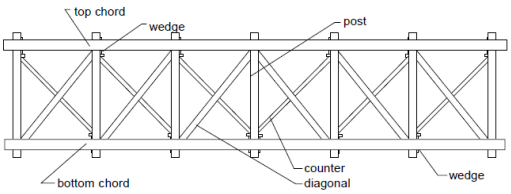

Figure 1.6: Long truss

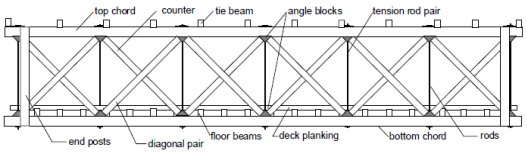

Figure 1.7: Howe truss
(US Department of Transportation Federal Highway Administration (2005))

Table 0.1: Number of surviving timber covered bridges
((US Department of Transportation Federal Highway Administration (2005))

Bridge Type	Number Surviving
Burr arch truss	224
Howe truss	143
Town lattice truss	135
Queenpost truss	101
Multiple kingpost truss	95

Many of the surviving covered timber bridges have been rehabilitated but their use has been changed from vehicular to pedestrian traffic in many cases. This can be due to the uncertainty in structural capacity of these bridges. To preserve the rich history of historical timber covered bridges and to potentially continue their use to carry vehicular traffic, a better understanding of the structure's performance and behavior must be understood. This can be accomplished by utilizing field tests and/or more accurate analytical methods. However, any analytical approach that can be used to analyze historical timber bridges must be capable of modeling most of the construction details as well as the most representative material properties of the timber. In addition, it is important to realize that it is not feasible to provide a generalized and simplified analytical modeling approach that can be utilized to analyze all the different types of covered timber bridges due to the varying geometry, the bridge type and the different construction of the joints. For example, each covered timber bridge system contains many eccentric connections, various load paths, a splice joint system, a load carrying system consisting of both truss and arch elements and the interaction between the trusses and their housing. These are among several reasons why one could easily expect to affect the structural behavior of these types of timber bridges.

According to a note in the Covered Bridge Manual, US Department of Transportation Federal Highway Administration (2005), there are inconsistencies with the assumptions of

traditional simple, static analysis of trusses that are frequently used to analyze covered bridges. For example, because of the way these bridges were constructed one needs to analyze the truss-arch elements of the bridge (will be referenced as main supporting element herein) as indeterminate structures. In this case, one should expect that the individual members of the main supporting element to experience combined axial and bending stresses. Neglecting this fact would easily lead to a specious conclusion that a historic timber covered bridge in some situations cannot withstand the required design load. Also, such conclusions can lead to inappropriate and unnecessary rehabilitation recommendations.

Due to the concern for the structural efficiency of historic covered wooden bridges, practicing engineers need a reliable way to analyze the structural behavior of covered bridges to determine the structural capacity and if further rehabilitation is necessary. By providing an effective way for practicing engineers to model and evaluate current covered timber bridges, their future presence in the national transportation system can be assured.

1.2 Scope of Research

The main goal of this research was to identify the most appropriate analytical modeling technique that can be used to improve analysis of historical covered timber bridges. The intersection and interconnection of structural members, impact of classic arch behaviors, behavior and interaction of bolster beams and floor systems are among the factors that must be included in the development of these models. In addition, all parameters that may affect the overall behavior of the analyzed historical timber bridges herein need to be clearly defined. The results of this analysis will allow bridge engineers to more accurately perform analyses needed to complete bridge evaluation and rating calculations.

CHAPTER 2: LITERATURE REVIEW

Limited research has been conducted that investigates the overall structural performance of historical covered timber bridges. For example, the effect of the splice joints which are used in the top and bottom chords of timer truss bridges were studied by others. This published information was utilized herein to assist in the development of the testing and the analytical modeling techniques. The findings of the published research that are related to the objectives of the study presented herein, i.e., the information on system behavior and the behavior of the splice joints of different covered timber bridge types are discussed below.

2.1 Overall Bridge Behavior

Studies have been completed across multiple types of bridges that have led to further questions of accurate analytical modeling approaches that provide practicing engineers an adequate method to determine the structural behavior of the bridge. Also, findings in such studies have provided regions within the bridge structure of which further studying is needed to determine their influence and response to the overall structural response to loading.

Lamar and Schafer (2004) along with Sangree (2006) evaluated the overall bridge behavior of multiple types of bridge structures. When comparing field test results to the developed analytical models, the studies determined that geometric properties such as the splice joints in the bottom chords should be evaluated to provide further explanation for the lack of convergence between the field and analytical results. Sangree evaluated many types of structures such as the queenpost, kingpost, Burr arch, and single and double-web Town lattice. Due to the focus on one bridge type within this study, only the work completed on Burr arch truss bridges will be evaluated.

2.1.1 Burr Arch Truss Bridge

Lamar and Schafer (2004) developed three analytical two dimensional beam models to evaluate the structural system behavior and efficiency of the Pine Grove Bridge located on the county line of Chester and Lancaster counties in southeastern Pennsylvania. Investigation included a model that evaluated the influence of the connection type, i.e., rigid or pin on the truss only portion of the bridge, another model that evaluated the structural

behavior of the arch only and a third that evaluated the combination of a truss-arch interaction within the model. The results of the Lamar and Schafer (2004) study revealed that excluding either of the two components, truss or arch, from the analytical model resulted in excessive deformation. These findings determined that the arch carries the load to the abutments and the truss provides some moment capacity. The design of the arch is efficient to carry uniform loads while it is inefficient to carry concentrated loads by itself. Thus, the truss system is designed to support the concentrated loads to ensure small deflections within the entire system. Lamar and Schafer recommended further studying to analyze the system behavior.

Experimental testing and analytical modeling was completed by Sangree (2006) for multiple types of bridges. The results determined that the bridges were not functioning as intended due to the differences in global deflections (field versus analytical) of the bridge system. To account for these differences, modeling adjustments were completed. Through analytical evaluation of the overall bridge, it was determined that details within the truss system were influencing the differences between the field testing and modeling results. Site investigation led to the finding that the lower mid-span diagonal to vertical connection was not seated properly to allow for full load transfer. Also, splice joints within the lower chord were evaluated. Through this system analysis, Sangree determined to evaluate other geometric considerations of the bridge to evaluate and quantify the differences between the values.

2.2 Scarf Joint Behavior

Finite element models were developed to further investigate the behavior of the specific components within the bridge structural system. Isolating specific portions of the bridge allowed the investigators to better understand and predict the behavior of the splice joint during the load transfer and the joint's influence on the entire structure's behavior. These investigations and findings also lend recommendations to practicing engineers for economical modeling techniques and also evaluation of joint strength. The two types of joints that have been evaluated by Sangree (2006) and Sangree and Schafer (2008) are for the bottom chord connection scarf joints; traditional and stop-splayed joints. Even though these

evaluated joints were not specifically within the Burr arch bridge discussed above (Lamar and Schafer (2004)), the findings were utilized to assist in determining the process of which field testing and analytical modeling would be completed within this study.

2.2.1 Halved and Tabled Traditional Timer Scarf Joint

Due to the deterioration of the joints present in many bridges such as the queenpost Morgan Bridge in Belvidere, Vermont, Sangree noted the difficulty in analyzing the behavior of the scarf joint with field testing alone. To further understand the joint behavior and effect in the overall bridge behavior, laboratory tests were completed on full-scale joints that replicated the field joint geometry. Below in Figure 2.1 is a graphical representation of the scarf joint utilized within Sangree's traditional scarf joint investigation.

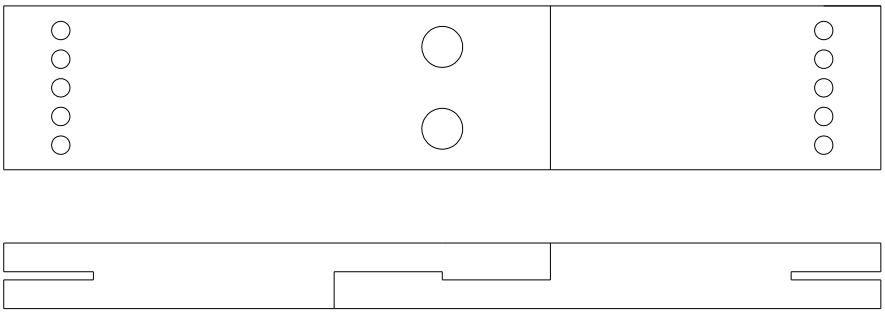

Figure 0.1: Graphical representation of scarf joint geometry (modeled after Sangree (2006))

Multiple data sets were collected to determine different structural behavior aspects of the joint. Many different displacements were evaluated such as axial, joint, contact and lateral. Also, axial strain across the cross sectional area of the contact region between the timbers was evaluated. From these test results, two distinct failure modes where seen within the joints: ductile and brittle.

From the data collected, the joint stiffness for each of the four tested samples was determined by the slope of the line of best fit. This line was determined through a linear regression calculation on the joint displacement data. The linear regression model included the data that was less than fifty percent of the ultimate strength and excluded initial nonlinearities within the data. The determined joint stiffness for each test was then used to verify the finite element modeling of the joint.

Before developing a finite element model, Sangree (2006) evaluated different aspects within the joint that would influence the structural behavior of the joint; joint axial stiffness, grain angle, and load eccentricity. Sangree evaluated the ability to express the stiffness of the joint through a simple axial spring model but was unable to verify the experimental stiffness value from lab testing to the calculated stiffness value. The scarf joint stiffness was determined through the basic stiffness equation where the stiffness is represented by k, the cross sectional area, A, modulus of elasticity, E, and the length, L, represented below by Eq. 2.1.

$$k = \frac{AE}{L} \qquad [\ 0.1]$$

First, the stiffness for a cross sectional area that is constant across the entire joint was determined. This calculated stiffness was magnitudes larger than the stiffness determined through testing. Due to this finding, Sangree determined that the deterioration of the joint reduced the cross section area at the area of the joint contact. To represent the joint, three springs with two different stiffness's were utilized, one that represented the value for the reduced cross sectional area at the joint location and the other for the unreduced cross sectional area. Below in Figure 2.2 is a graphical representation of the spring model that represents the different cross sectional values of the joint. The stiffness of the joint is then calculated by utilizing the traditional equation for springs within a series. Recalculating the joint stiffness including the reduced cross sectional area also provided a larger calculated value of the joint stiffness than experimental testing found. Sangree (2006) concluded that due to the inability to explain the joint stiffness with a simple axial spring model, bending due to eccentric loading must be present within the joint.

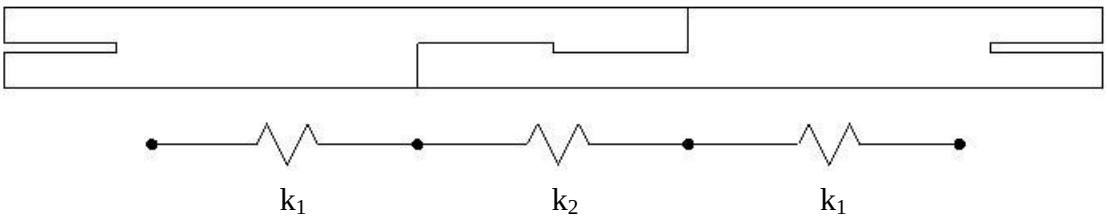

Figure 2.2: Spring model for scarf joint (modeled after Sangree (2006))

Also from the previously completed overall bridge behavior finding, the stiffness behavior of having a spliced chord member in the presence of the scarf joint was evaluated. Even with this variation in the geometry in determining the joint stiffness, little additional stiffness is provided to the calculation from the splice member making its absence from the model insignificant.

Within the geometry of the scarf joint, bending was found to be present in the joint due to the eccentric load transfer. An illustration of this eccentric that develops within the joint due to the transfer of the load through the joint's geometry is seen in Figure 2.3.

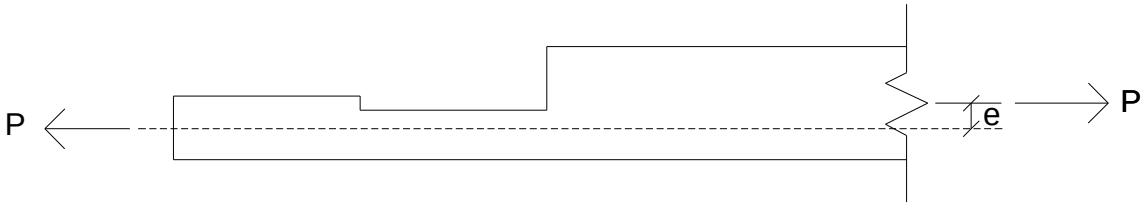

Figure 0.3: Eccentric load transfer of scarf joint

Sangree (2006) evaluated two methods to determine the eccentricity within the joint. The first method involved determining the resultant of all three strain gauge readings across the length of the joint contact. Then determinacy of the eccentric value was done by calculating the equivalent resultant axial strain value minus the distance from the resultant to the contact surface of the joint. Conclusions from this method included that the eccentricity was relatively constant during linear elastic loading and that the grain orientation does not influence the eccentricity of the joint. The second method utilizes the position transducer data from the laboratory testing that measured the lateral displacement of the joint. Method

two assumes that the joint may be idealized as a cantilever beam. Within this cantilever beam model, simple elastic beam mechanics (Eq. 2.2) can be utilized to develop the quantity of moment that was applied to the joint at mid-length of the joint due to the eccentricity.

$$\frac{dv}{dx} = \theta_{bending} = \frac{ML}{EI} \qquad [2.2]$$

Deflection from each of the three position transducers was used to determine the angle of bending. By knowing this value from testing, Eq. 2.2 above may be rearranged to solve for the moment value. Then for each test, the calculated moment was plotted against the load where a line of best fit was the placed. From the line, the inverse slope of the line is the eccentric distance for the specific joint. From knowing the eccentricity of the joint, an engineer has a greater capacity to calculate the maximum stress within the cross section. With the tests, the moment was determined to be a linear function of the load implying a constant eccentricity. (Sangree (2006)).

From the experimental results Sangree (2006) and Sangree and Schafer (2008) concluded that the limit state for the splice joint was dependent on the grain angle of the shear plane within the joint. This finding provided an explanation for the differences between the experimental and analytical results. This failure was determined to lie between the maximum principal strain and principal strain direction near the area of contact within the splice joint. The analysis showed that with an increasing grain angle, the limit state changes from shear failure parallel to the grain to tension failure perpendicular to the grain. Due to the current methods utilized in evaluating scarf joints, a limit state due to tension failure perpendicular to the grain angle was not evaluated.

Sangree (2006) developed multiple solid element three dimensional analytical models to validate the laboratory testing conclusions. These three dimensional models only incorporated the scarf joint and a small vicinity of the chord member near the scarf joint with axial load applied with respect to the joint. From the results of this model and with comparison to the laboratory findings, Sangree (2006) found that when the grain angle orientation increases, the probability of failure due to excessive tension perpendicular to the grain also increases. Due to this failure, Sangree (2006) non-dimensionalized for the effect

of grain orientation on the axial stiffness and eccentric to draw conclusions. In all, Sangree's analytical models further assisted in determination of the correct material model which should be utilized within the scarf joint. Sangree (2006) concluded that utilizing a transversely isotropic model in the linear elastic region was sufficient to validate results between analytical and laboratory tests. Also, when evaluating the stiffness of the joint with respect to the chord member, Sangree (2006) and Sangree and Schafer (2008) concluded that the scarf joint stiffness is much less relative to the stiffness of the chord member.

2.2.2 Stop-Splayed Scarf Joint

Much like the above discussed scarf joint, Sangree (2006) and Sangree and Schafer (2008) evaluated the stop-splayed timber scarf joint with the presence of a key between the timber members. The major difference between the traditional scarf joint discussed previously and the stop-splayed scarf joint is the increased contact area of the joint along with the presence of a key between the timber members (see Figure 2.4). The same type of laboratory testing was completed for this type of scarf joint as was done for the previous scarf joint; full scale joints with geometry replicated from the in-field joint geometry. Also, as was completed with the previous joint, three dimensional finite element models were developed and the results compared to the laboratory findings.

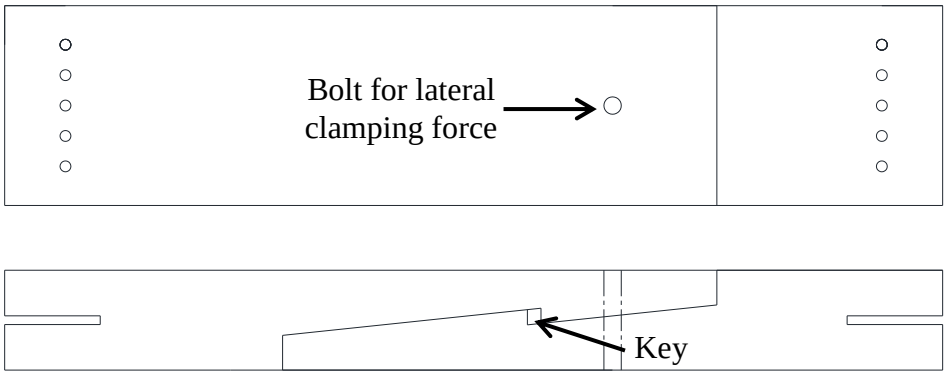

Figure 2.4: Graphical representation of stop-splayed scarf joint geometry (modeled after Sangree (2006))

From the laboratory testing evaluations, Sangree (2006) concluded that the presence of the key influences the behavior of the joint. The key provides an additional eccentricity to

the load transfer of the joint when compared to the key's exclusion. This additional eccentricity that is created due to the key can only be resisted by the lateral clamping force of the bolt within the scarf joint. When evaluating the failure mechanisms of this joint, Sangree (2006) and Sangree and Schafer (2008) found that without the application of the clamping force, the limit state of the stop-splayed scarf joint was reduced to "key rolling": the axial stiffness of the entire joint is reduced to only the stiffness of the isolated key. With the inclusion of the clamping force within the evaluation of the joint, the scarf joint has a completely different limit state and localized behavior. The joint will fail due to shear parallel to the grain which in turn relates to an axial stiffness of the joint greater than without the clamping force due to the lateral confinement of the key.

With respect to the analytical evaluation, similarly to the traditional scarf joint, for the stop-splayed scar joint solid element three dimensional models which included modeling the contact surfaces between the faces of the timber members in the vicinity of the joint were completed. Similar conclusions were established for the stop-splayed joint as were for the traditional joint.

As discussed above, no analytical studies carried out by other researchers took into account the effects of the scarf joint within the behavior of the overall bridge. Thus, the study presented herein focused on developing a simple but accurate analytical model that is capable of evaluating the overall structural behavior of Burr arch truss bridges. These models included the geometry of the structure along with the effect of the joints between the vertical, diagonals, top and bottom chords of the trusses. The developed analytical models were calibrated using field test results.

CHAPTER 3: FIELD TESTING OF COVERED BRIDGES

To better understand the structural behavior of covered timber bridges and to validate the use of analytical modeling, a series of a single bridge type was selected to be studied. In the work presented herein, three currently in service Burr arch truss bridge type located in southern Indiana were evaluated through field testing and analytical evaluation. The collected field test results of global displacements and strain values were recorded for different structural timber elements within the bridge system. This data was used to assess the most appropriate modeling of the truss-arch system for a finite element analysis.

3.1 Bridge Descriptions

Even though each of the three evaluated bridges has similarities with respect to geometric properties, each is very distinct from the other. Below is a brief discussion of each of the three bridges that were selected. These bridges are the Zacke Cox Bridge, Portland Mills Bridge and Cox Ford Bridge, which were all located in Parke County, Indiana.

3.1.1 Zacke Cox Covered Bridge (BR. #63)

The location of the Zacke Cox Bridge and surrounding Parke County, Indiana is illustrated in Figure 3.1. The Zacke Cox Bridge allows traffic to cross the Rock Run Creek which is located on the Tickridge Road approximately 0.5 miles northwest of Fisher Road. Elevation and end view photographs of the bridge are shown in Figure 3.2. The Tickridge Road is an unpaved road with a low average daily traffic (ADT) count. The bridge was originally built in 1908 by Joseph A. Britton and its roof and deck were replaced in 1989, the deck was again replaced in 1991 and the bridge was restored in 2002 (Parke County Website Zacke Cox Bridge (2011)).

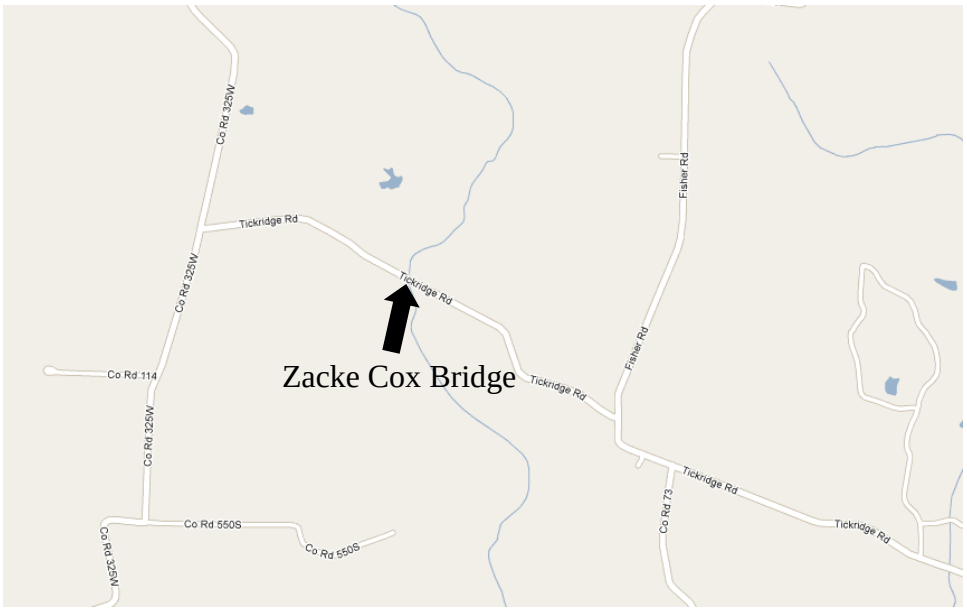

Figure 3.1: Location of the Zacke Cox Bridge, BR 63, in Parke County, IN

Figure 3.2: Different views of the Zacke Cox Bridge

The Zacke Cox Bridge is a one lane, single span, simply supported double Burr arch truss with a measured end bearing to end bearing length of the main supporting element to be 51 ft. The truss consists of rectangular parallel chords, concentric arches enclosing the truss, two member lower chords, one member upper chords, one member diagonals and one member verticals. Schematics of the truss elevation and plan views are provided below in Figures 3.3, 3.4 and 3.5. Currently, the bridge is rated and posted for a thirteen ton load limit. (Clark Dietz Bridge No. 63 (2009)).

Due to the rehabilitation efforts completed on the bridge in 2002, many of the original timber members were replaced with new sawed or glued-laminated timbers. For example, the stringers and floor beams were replaced with glulam timbers due to their greater allowable bending stress capacity over sawn timber (Loiselle (2011)). Part of the rehabilitation effort also included the change in the location and the number of the floor beams and stringers (Indiana Department of Transportation (2001)). Finally, where deteriorated members of the truss or arch were seen, they were replaced with new sawed timbers.

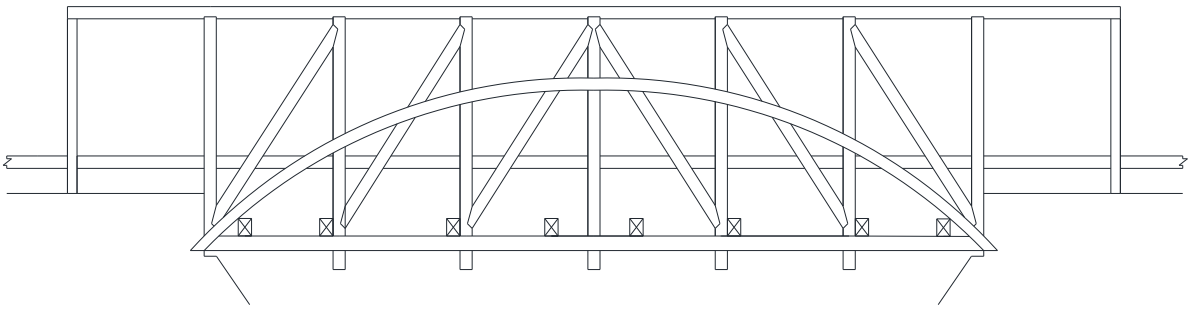

Figure 3.3: Elevation view of the Zacke Cox Bridge

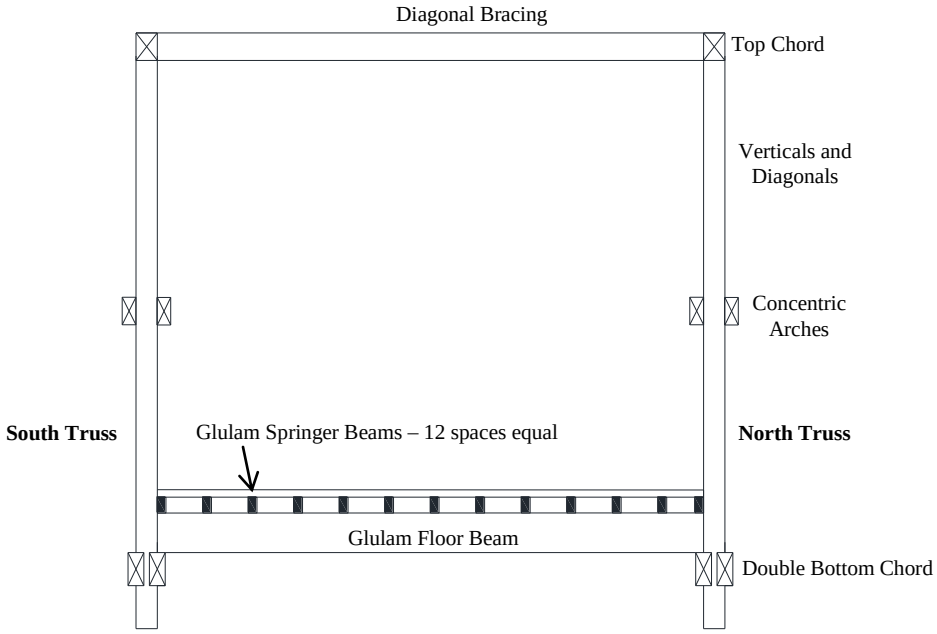

Figure 3.4: Cross sectional view of structural components

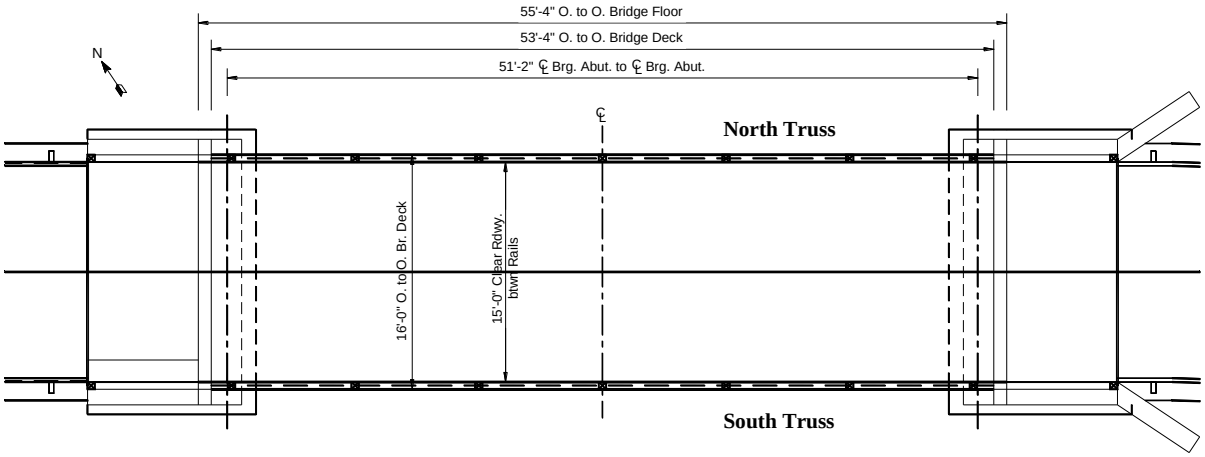

Figure 3.5: Plan view of the Zacke Cox Covered Bridge, Parke County, IN

There are many structural components that comprise the Zacke Cox Bridge. Table 3.1 summarizes the approximate dimensions of each structural member used within the bridge and analytical models. The total height from the bottom of the bottom chord to the top of the top chord was measured to be 14.6 ft. with an average truss panel spacing of 8.4 ft. All the connections between the timber members i.e., the connection between the two arches and vertical were accomplished using either a single or series of bolts.

Table 3.1: Structural member dimensions of the Zacke Cox Bridge

Structural Member	Base Length (in.)	Height Length (in.)
Bottom Chord (2)	5.5	11.5
Floor Beam (new)	10.5	13.8
Verticals	7.5	9.5
Diagonals	7.5	7.5
Arch (2)	4.75	9.5
Top Chord	7.5	9.8

Due to the natural limitations of timber, infinite lengths of timbers are not available to span the entire length of the bottom or top chords of the truss structure. Instead, splices are used to connect two timber members together. The Zacke Cox Bridge utilizes single headed hook fishplate and iron shoe splice joints within the bottom chord (Marston (2006)). There are two such splice joints in the Zacke Cox Bridge. These joints are located one on each side of the center as shown in Figure 3.6 below. A detailed plan view of the bottom chord splice joint that is within Figure 3.6 is illustrated below in Figure 3.7.

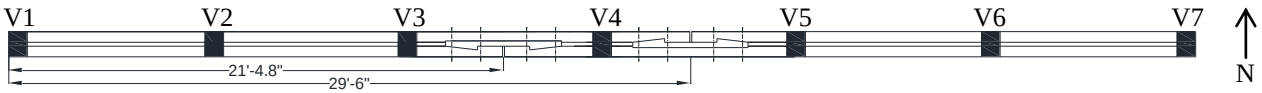

Figure 3.6: Plan view of bottom chord with location of splice joints in the south truss

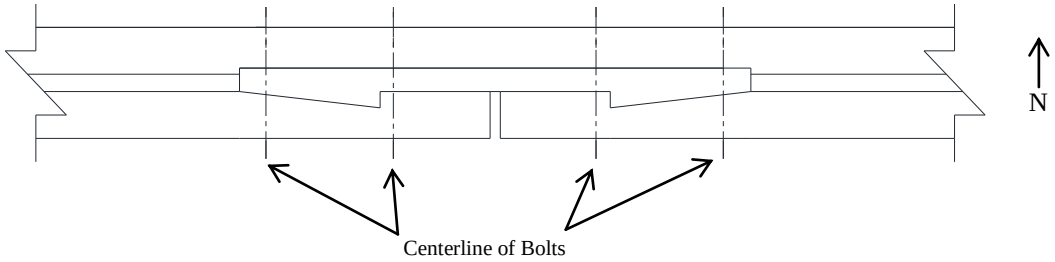

Figure 3.7: Plan view of the south truss bottom chord splice joint detail between truss panels 3 and 4

3.1.2 Portland Mills Covered Bridge (BR. #155)

The Portland Mills Bridge (also referenced as Bridge No. 155) is located on County Road 650 approximately 0.2 miles east of Saddle Club Road in Parke County, Indiana. County Road 650 is an unpaved road with a low ADT count. Figure 3.8 shows the location

of the structure and the surrounding Parke County area. The Portland Mills Bridge allows traffic to cross the Little Raccoon Creek. Elevation and end view photographs of the bridge are shown in Figure 3.9.

Figure 3.8: Location of the Portland Mills Bridge, BR 155, in Parke County, IN

Figure 3.9: Different views of the Portland Mills Bridge

Out of the covered bridges in Parke County, the Portland Mills Bridge is one of the oldest. It was built in 1856 by Henry Wolfe. The bridge originally crossed the Big Raccoon Creek in Portland Mills but was later moved in 1961 to replace the burned down Dooley Station Bridge. The floor stringers and roof were replaced in 1909. Due to the deterioration of some timber members, missing sections of the roof and siding and portions of the structure

that previously experience damage due to fire, the bridge was closed in 1982. From 1991 to 1996, rehabilitation efforts to bring the bridge back to its original state were completed to avoid collapse of the structure. (Parke County Website Portland Mills Bridge (2011)).

The Portland Mills Bridge is a one lane, single span, simply supported double Burr arch truss. The truss consists of two rectangular parallel bottom chord members, double concentric arches enclosing the truss, one member upper chords, one member diagonals and one member verticals. The measured end bearing to end bearing length of the main supporting element is 120 ft. Schematics of the truss elevation view and plan view are provided below in Figures 3.10, 3.11 and 3.12. Currently the bridge is rated and posted for a thirteen ton load limit. (Clark Dietz Bridge No. 155 (2009)).

Over time, multiple rehabilitation efforts have been completed on the Portland Mills Bridge. Throughout these improvements of the bridge, some characteristics of the original structure have been modified. These rehabilitation efforts included the replacement of the timber floor beams and stringers with glue-laminated timbers. Also, the entire bottom chord along with portions of the top chord and a few diagonal and vertical members located at each end of the structure were replaced with new sawn timbers. (Indiana Department of Transportation (1995)).

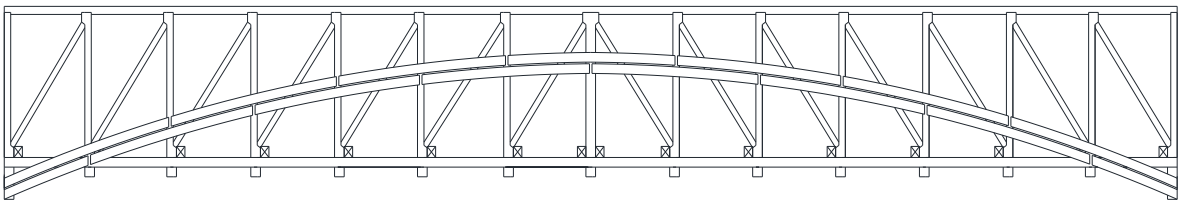

Figure 3.10: Elevation view of the Portland Mills Bridge

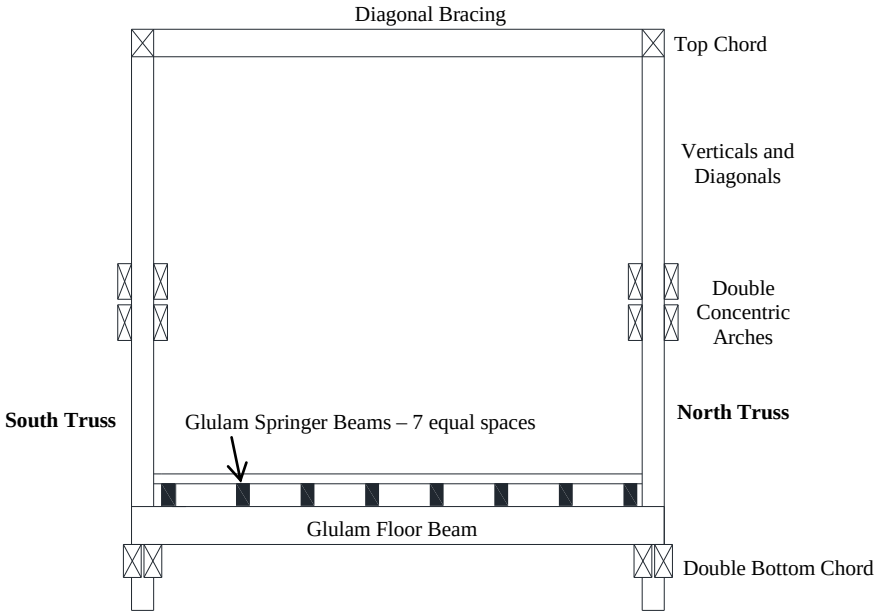

Figure 3.11: Cross sectional views of structural components

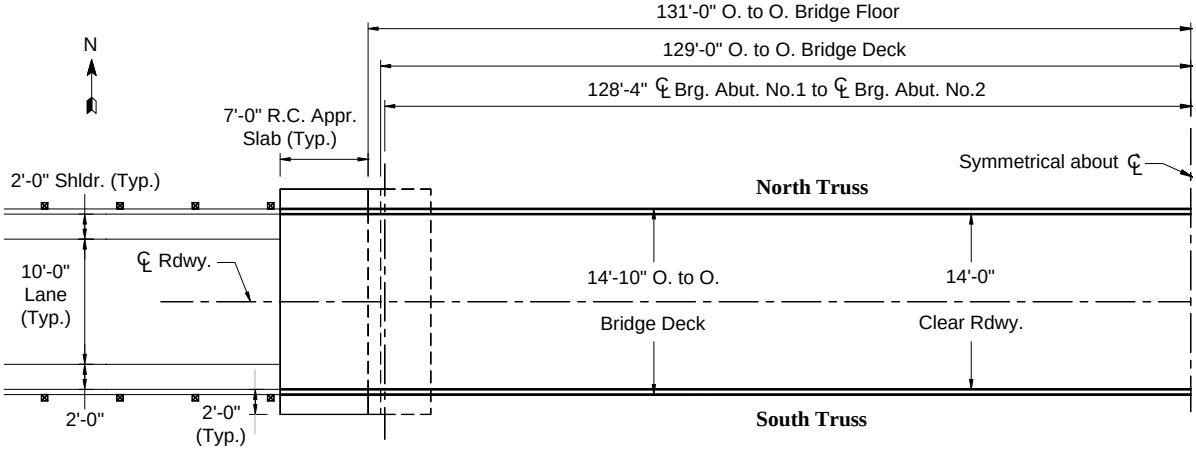

Figure 3.12: Plan view of the Portland Mills Bridge, Parke County, IN

Similar to the Zacke Cox Bridge, the Portland Mills Bridge has many structural components which comprise the overall structure. Table 3.2 summarizes the dimensions of each structural member as approximately measured in the field. The total height from the bottom of the bottom chord to the top of the top chord was measured to be 16.7 ft. and an average truss panel spacing of 8.7 ft. The connection between structural timber members, i.e. the connection between the multiple arches and vertical members, is completed by using either a single or series of bolts.

Table 3.2: Structural member dimension of the Portland Mills Bridge

Structural Member	Base Length (in.)	Height Length (in.)
Bottom Chord (2)	6.50	12.00
Floor Beam	10.50	13.75
Verticals	8.00	8.00
Diagonals	8.00	7.00
Arch (2)	5.00	13.00
Top Chord	8.00	10.00

Due to the sheer clear span length of the bridge, multiple stop-splayed splice joints were necessary both in the bottom and top chord members. For the bottom chord, a total of six stop-splayed splice joints were used within a single main supporting element. The location of these joints along with a detailed plan view illustration of the joint may be referenced in Figures 3.13 and 3.14, respectively. Within the top chord, a total of four stop-splayed splice joints were used within a single main supporting element. Figures 3.15 and 3.16 represent the elevation view of the entire top chord along with a detailed elevation view of the splice joint, respectively.

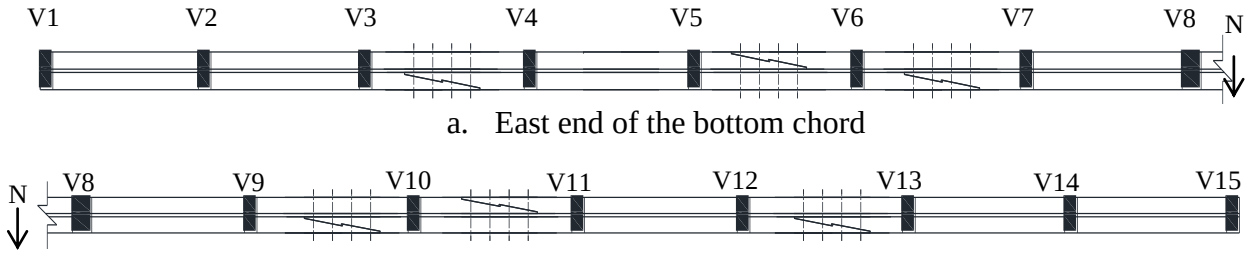

a. East end of the bottom chord

b. West end of the bottom chord

Figure 3.13: Plan view of bottom chord with location of splice joints

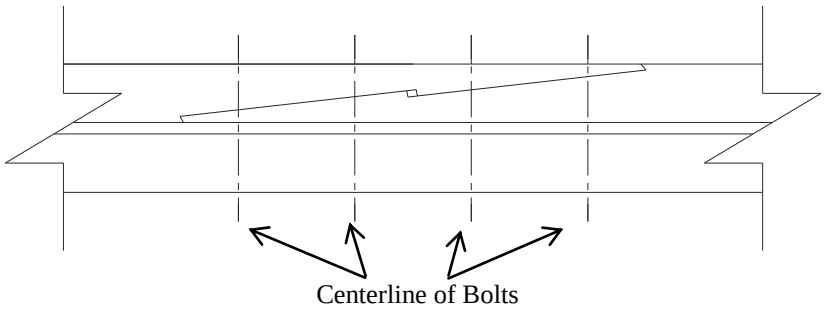

Figure 3.14: Plan view of bottom chord splice joint detail

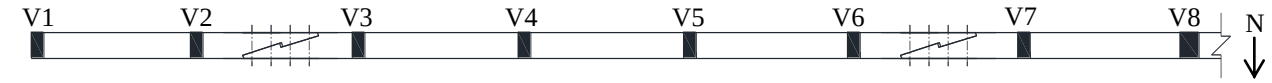

a. East end of the top chord

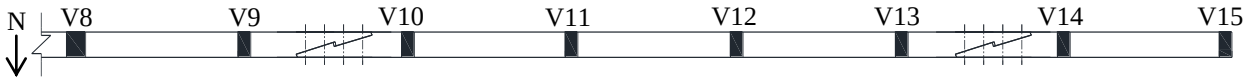

b. West end of the top chord

Figure 3.15: Elevation view of top chord with location of splice joints

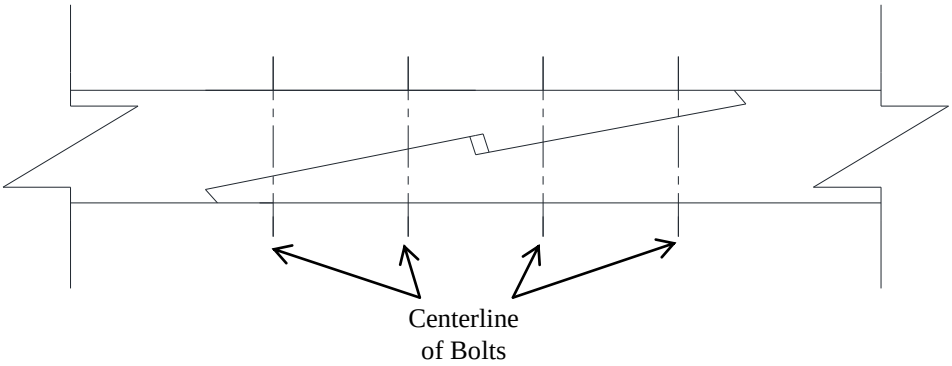

Figure 3.16: Elevation view of top chord splice joint detail

3.1.3 Cox Ford Covered Bridge (BR. #227)

The Cox Ford Bridge (also referenced as Bridge No. 227) is located on Cox Ford Road and allows traffic over the Sugar Creek located east of US 41, north of Indiana 47 and west of Turkey Run State Park. Cox Ford Road is an unpaved road with a low ADT count. The location of this bridge along with the surrounding area is located below in Fig. 3.17. Elevation and end view photographs of the bridge are shown in Fig. 3.18. (Parke County Website Cox Ford Bridge (2011)).

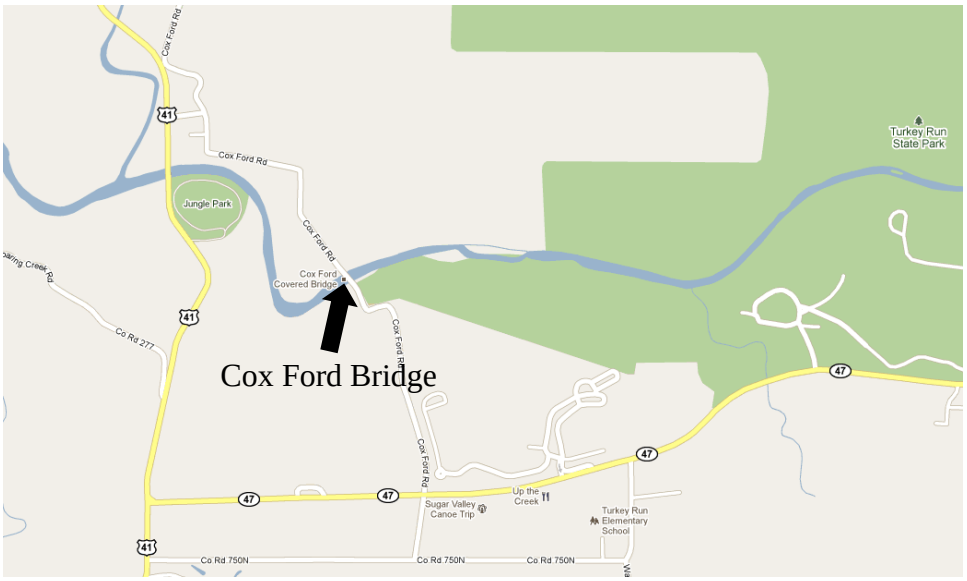

Figure 3.17: Location of the Cox Ford Bridge, BR 227, in Parke County, IN

Figure 3.18: Different views of the Cox Ford Bridge

The structure was originally built in 1913 by Joseph A. Britton to replace an iron bridge that had been destroyed in a flood. Repairs and rehabilitation have been completed on this structure both in 1975 and 1991. There are currently no plans available of either the original or rehabilitation projects. Thus, only field measurements were available for analytical evaluation. (Park County Website Cox Ford Bridge (2011)).

The Cox Ford Bridge is a one lane, single span, simply supported double Burr arch truss with a measured bearing end to bearing end length of 183 ft. The truss consists of rectangular parallel chords, double concentric arches enclosing the truss, two member bottom chords, one member upper chord, one member diagonals and one member verticals. Schematics of the truss elevation and plan view are provided below in Figures 3.19 and 3.20. Currently the bridge is rated and posted for a five ton load limit. (Clark Dietz Bridge No. 227 (2009)).

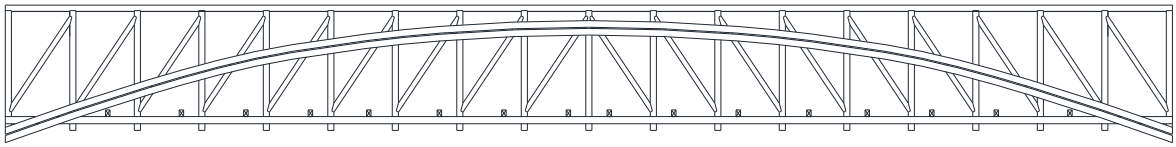

Figure 3.19: Elevation view of the Cox Ford Bridge

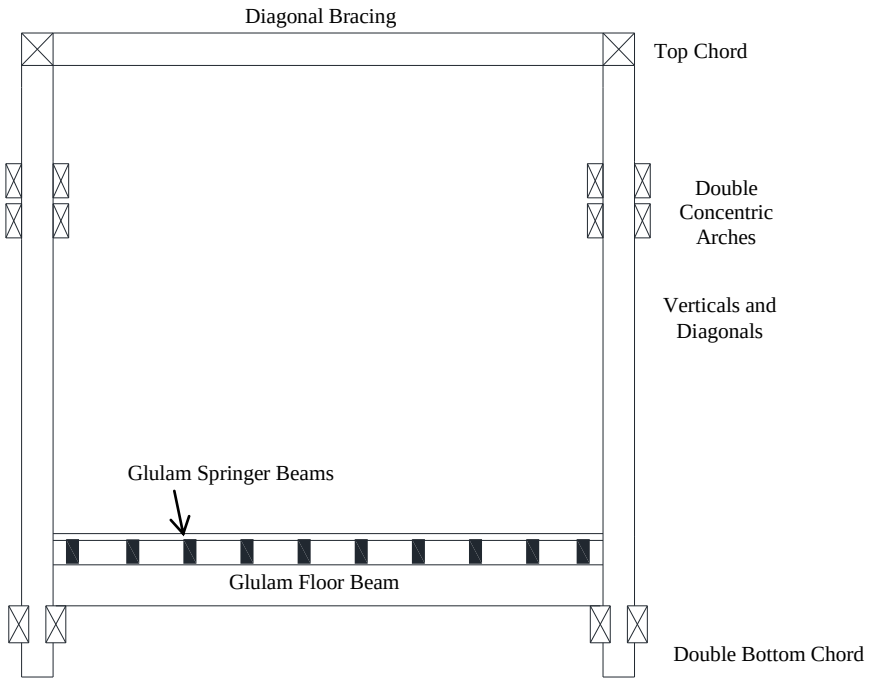

Figure 3.20: Cross sectional views of structural components

Table 3.3 below contains dimensions of each structural member used within the analytical model as measured in the field. The total height from the bottom of the bottom chord to the top of the top chord was measured to be 17.8 ft. and an average truss panel spacing of 9.75 ft. Just as discussed in the previous two bridges, the connections between timber members were accomplished by the utilization of either a single or series of bolts.

Table 3.3: Structural member dimension of the Cox Ford Bridge

Structural Member	Base Length (in.)	Height Length (in.)
Bottom Chord (2)	7.00	13.00
Floor Beam	8.00	12.00
Verticals	9.00	11.00
Diagonals	9.50	9.50
Arch (2)	5.50	12.00
Top Chord	9.25	11.38

Due to the overall span length of the structure with no intermediate supports, nine splice joints were used within one main supporting element. As can be seen in Figure 3.21, the splice joints were placed in every other truss panel with alternating orientation. A detailed plan view of the splice joint geometry may be referenced in Figure 3.22. In the other truss panels, there are timbers that act as spacers between both of the bottom chord members to ensure that the bottom chord members can minimally move out of plane from each other. A detailed plan view of the splice block detail in the bottom chord may be seen in Figure 3.23.

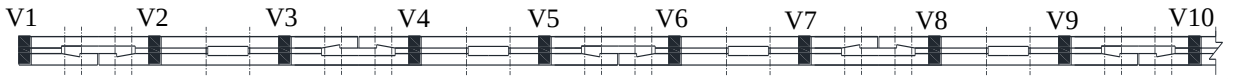

a: South end of the bottom chord

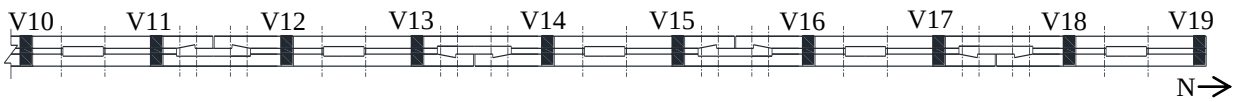

b: North end of the bottom chord

Figure 3.21: Plan view of the bottom chord with location of splice joints

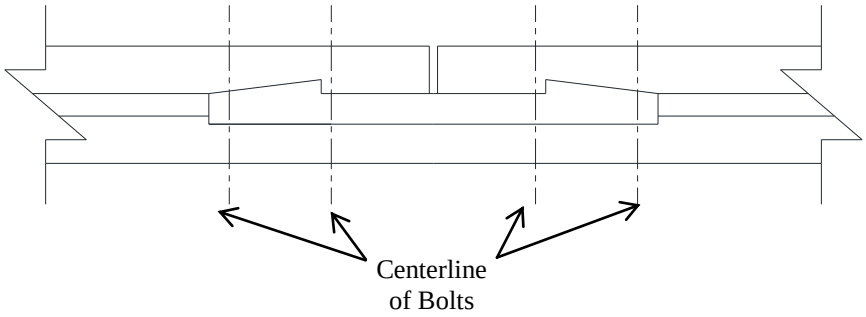

Figure 3.22: Plan view of bottom chord splice joint detail

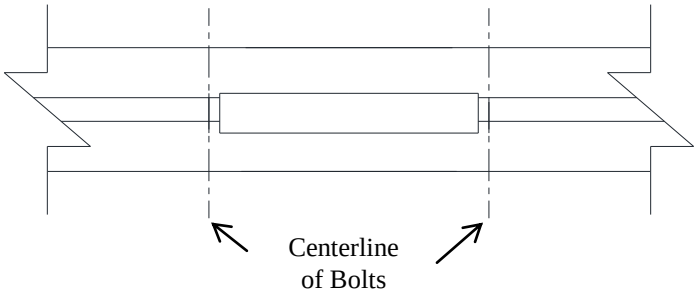

Figure 3.23: Plan view of bottom chord splice block detail

3.2 Field Testing

Field testing of each structure included the use of a vehicle of known weight distribution along with instrumentation to measure the response of the bridge to vehicular loading. In the collection of the data, both displacement and strain values were measured across multiple locations on each structure. On the Zacke Cox and Cox Ford bridges, two different vehicles with different total weights were driven across for data collection while only the smaller of the two vehicles was used on the Portland Mills Bridge. The test vehicle weight for testing of each bridge was limited by the posted weight limits for each bridge.

3.2.1 Instrumentation

3.2.1.1 Displacement Measurements

To measure the displacement values, an Optim Megadac data acquisition system (DAS) was used along with a Dell laptop computer which ran the TCS software to provide

communication between the Megadac and ratiometric displacement transducers. The transducers that were used were Celesco and Unimeasure. With respect to the collection of strain data, the Bridge Diagnostics Inc. (BDI) data acquisition system was used along with the BDI strain transducers.

Four global displacement measurements were completed on each bridge. Two transducers were placed at the mid-span point, one on each main supporting element, and the other two were placed at the quarter-span point in a similar fashion (Figure 3.24.a). Also, at each splice joint which was selected to be evaluated in the field, two or three displacement transducers were used to measure the movement both longitudinal and transverse of the joint (Figure 3.25.b).

a. Displacement gauges and tripods for mid-span and quarter-span deflection measurements on both trusses

b. Displacement transducers for splice joint (i.e., top chord) for deflection in the longitudinal and transverse directions with respect to the orientation of the bridge structure

Figure 3.24: Typical displacement transducer testing set up

3.2.1.2 Strain Measurements

Strain measurements were taken at many different locations along the bridge's structure. In general, measurements were taken at the splice joint locations in the bottom and top chords, at mid-span of the mid-span floor beam, in the verticals around mid-span, diagonals near the bridge mid-span and at multiple arch locations (Figure 3.25). Each strain gauge was connected to the timber member with two zinc-plated steel hex washer head sheet metal screws, slotted, No. 12 size and 1.5 in. in length.

Figure 3.25: Typical strain transducer testing set up (top left is of multiple verticals, top right is underside of double concentric arch and vertical, bottom left is of multiple verticals and diagonals and bottom right of a splice joint in the bottom chord)

3.2.2 Vehicles Used for the Field Test

For testing, two vehicles were provided by the Parke County Public Works Department. The first vehicle was a two axle water truck (Figure 3.36) and the second a two axle dump truck (Figure 3.37). Table 3.4 provides the axle weight and axle center to center measured distance for each vehicle. The trucks were driven across the bridge down the center of the structure at a slow rate, approximately five miles per hour, to stimulate static loading conditions.

Figure 3.36: Images of different views of the small truck testing vehicle

Figure 3.37: Images of different views of the large truck testing vehicle

Table 3.4: Axle weights of each truck used in testing

	Front Axle (lbs)	Back Axle (lbs)	Axle Center to Center Distance (in.)
Small Truck (Water)	3,960	6,480	169
Large Truck (Dump)	9,340	9,460	121

For further details related to the field testing procedure and results, the reader is referred to a report that is in preparation and will be submitted to the FPL under the following project number; Covered Bridge Rating through Load Testing Project No. 10-JV-11111133-013.

CHAPTER 4: FINITE ELEMENT ANALYSIS

4.1 Analytical Methodology

For each of the three Burr arch bridges described previously, the general purpose finite element program, ANSYS, was utilized to complete the necessary analysis (ANSYS (2011)). Due to the overarching goal of providing practicing engineers a simple and appropriate modeling technique to model the structural behavior of these types of bridges, only one of the two main supporting elements of the bridge was evaluated. By this simplification, each of the bridge models does not include the influence of the bridge deck, floor beams, stringers, siding or roofing.

4.2 Finite Element Modeling

Within the analytical evaluation of the main supporting element for each of the bridges, both two and three dimensional finite element stick models were developed to model the truss-arch interaction. Due to the concern that bridge engineers could potentially evaluate these types of structures as two dimensional stick models excluding the as built conditions and as a pure truss, these scenarios were evaluated and compared to the field test results. The three dimensional stick model was developed to incorporate the as built conditions of the bridge such as the multiple splice joint locations along with the double chord members; bottom chord and arch.

4.3 Elements

Both two and three dimensional finite element analyses were completed using the ANSYS software. Due to the different dimensions of idealization, the ANSYS beam elements that were used within each model type differed. For the two dimensional finite element stick model idealizations, a two dimensional beam element was used to model all the timber members; top and bottom chord, verticals, diagonals and arch. The element that was selected in the ANSYS element library is referred to as BEAM3. This element has three degrees of freedom at each node; translations in the x and y directions and rotation about the z-axis. While for the three dimensional models stick model idealizations, the three dimensional beam element, referred to as BEAM4 in the ANSYS element library, was

utilized. Unlike BEAM3, the BEAM4 element has a total of six degrees of freedom at each node. Thus, in addition to the translations and rotations of the BEAM3 element, the BEAM4 element also allows for translation in the z direction and rotation about the x and y axes. Also, unlike BEAM3, BEAM4 is capable of representing torsional responses within the model. To represent the rotational capacity between the timber member connections, a unidirectional combination element with a nonlinear generalized force-deflection capability was utilized and is referred to in the ANSYS element library as COMBIN39. At each node, there is one degree of freedom that represents the translation or rotation about a nodal coordinate axes, pressure or temperature. Lastly, constrained equations were used to ensure that the structural timber members that are connected on the bridge moved in unison. (ANSYS (2011)).

Within the development of the models for each bridge, an iterative modeling process was completed on the first bridge, the Zacke Cox Bridge. Through the comparison between the field data and analytical models, the most representative modeling approach was developed and implemented on the following two bridges; the Portland Mills Bridge and the Cox Ford Bridge.

4.4 Measured Relative Longitudinal and Transverse Splice Joint Deflections

4.4.1 Zacke Cox Bridge

Below in Figure 4.1 is a picture of the bottom face of one of the bottom chord south truss's splice joint with the field displacement instrumentation. Table 4.1 lists the field recorded maximum deflection values, positive and negative, seen in both the bottom chord north and south truss joints. The north truss splice joint has similar displacement instrumentation as that shown in the south truss.

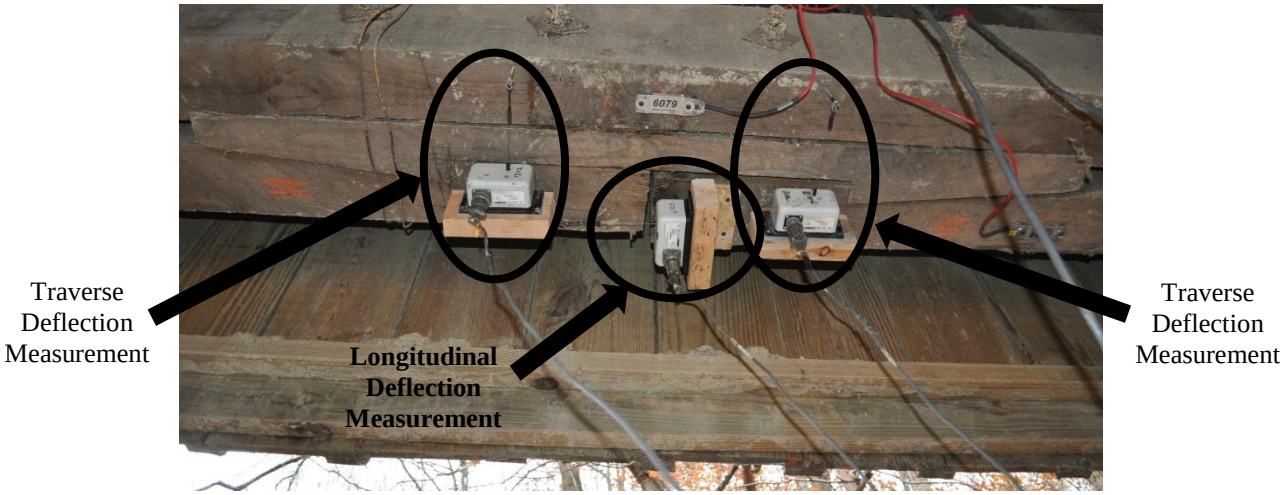

a. Photograph of the bottom face of the bottom chord displacement measurements

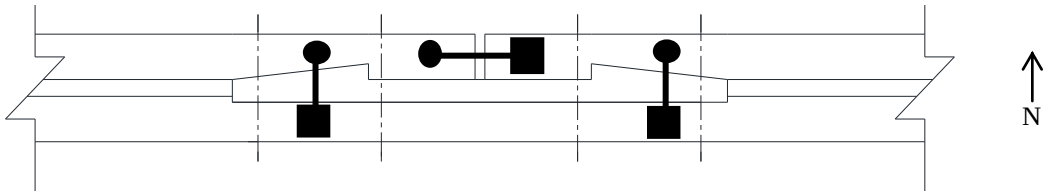

b. Sketch of the elevation view representing the longitudinal and transverse deflection measurements

Figure 4.1: Splice joint deflection instrumentation for the south truss on the Zacke Cox Bridge

Table 4.1: Field splice joint deflection results for the Zacke Cox Bridge – small and large truck

		Small Truck		Large Truck	
Truss	Displacement	Maximum Positive Deflection (in.)	Maximum Negative Deflection (in.)	Maximum Positive Deflection (in.)	Maximum Negative Deflection (in.)
South Truss	Transverse to the bridge	0.003	0.001	0.003	0.002
		0.002	0.000	0.001	0.001
	Longitudinal to the bridge	0.007	0.002	0.014	0.003
North Truss	Transverse to the bridge	0.003	0.001	0.005	0.001
		0.001	0.001	0.002	0.001
	Longitudinal to the bridge	0.010	0.000	0.022	0.001

4.4.2 Portland Mills Bridge

Below in Figures 4.2 and 4.3 are images of the in-situ and sketches of the deflection gauge configuration and measurements for the bottom chord and top chord, respectively. Unlike the splice joint geometry in the Zacke Cox Bridge, the stop-splayed splice joint with a key was present within the Portland Mills Bridge. Due to this, only one measurement was made in the transverse direction of the bridge for both the bottom and top chords. Table 4.2 lists the maximum field recorded positive and negative deflection field values for both directions in both chord members; top and bottom.

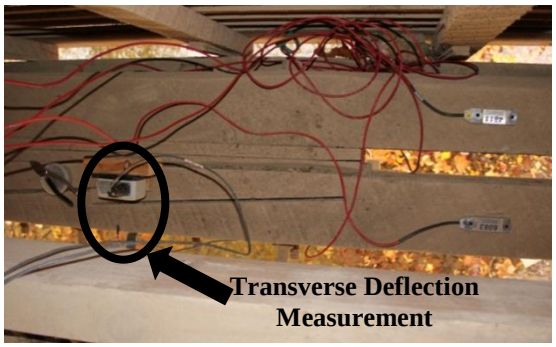

a. Transverse deflection top of chord

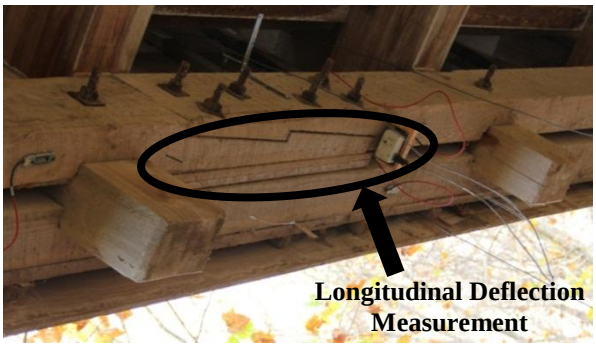

b. Longitudinal deflection bottom of chord

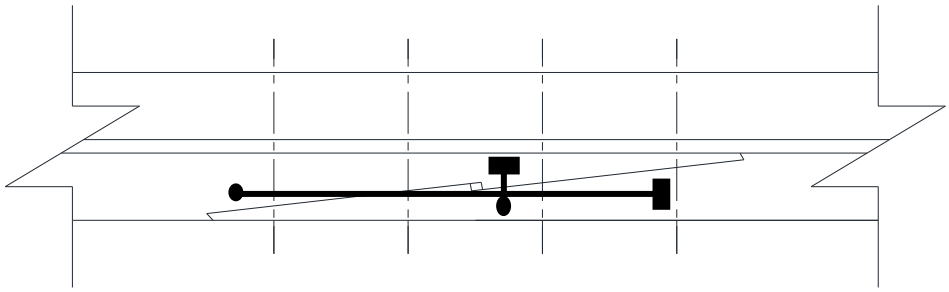

c. Sketch of the plan view representing the longitudinal and transverse deflection measurements

Figure 4.2: Bottom chord splice joint deflection instrumentation for the south truss on the Portland Mills Bridge

a. Photograph of the elevation view of the top chord displacement measurements

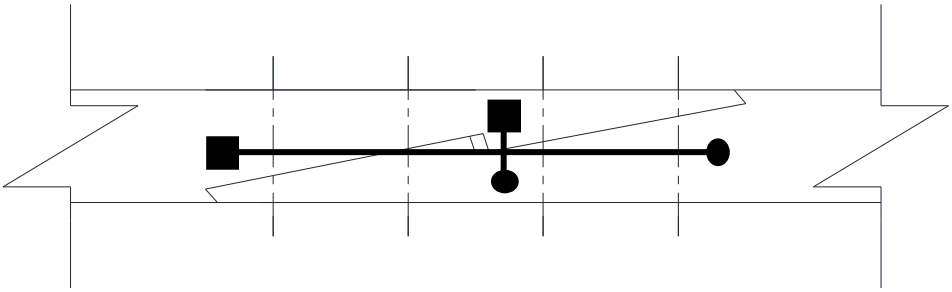

c. Sketch of the elevation view representing the longitudinal and transverse deflection measurements

Figure 4.3: Top chord splice joint deflection instrumentation for the south truss on the Portland Mills Bridge

Table 4.2: Field splice joint deflection results for the Portland Mills Bridge – small truck

			Small Truck	
Truss	Chord Member	Displacement	Maximum Positive Deflection (in.)	Maximum Negative Deflection (in.)
South Truss	Bottom Chord	Longitudinal	0.002	0.003
		Transverse	0.001	0.002
	Top Chord	Longitudinal	0.001	0.003
		Transverse	0.002	0.002

From Tables 4.1 and 4.2, one may notice that there is minimal deflection in both longitudinal and transverse directions for each bridge splice joint. With a relatively small movement of the joint in both directions due to the applied loads, one may conclude that the splice joint in the bottom chord and top chord members have a relatively high longitudinal and transverse stiffness. Therefore, it was concluded that it is appropriate to constrain the members of both sides of the splice joint to move together in the longitudinal and transverse directions.

4.5 Zacke Cox Bridge

4.5.1 Finite Element Models

For the Zacke Cox Bridge, both two and three dimensional stick models were developed to determine the most representative modeling approach for the overall bridge behavior in response to vehicular loading.

4.5.1.1 Two Dimensional Modeling

The two dimensional stick models that were analyzed are shown in models I through VII. In these models the two arches and the two members of the bottom chord of each main supporting element were each modeled as one element with an equivalent cross sectional area and moment of inertia. Figures 4.4.a through 4.4.g summarize the different alternatives that were used to model the connections between the different elements. In these illustrations, the dark filled circle represents the modeling of a rigid connection, i.e., connecting all members intersecting at a joint using a common node. This idealization was employed in models I, II and III. In model I (Figure 4.4.a), eccentricity of the joints was not considered. Shown in model II (Figure 4.4.b) are the eccentricities that are caused by the construction between the diagonal and the vertical members. The difference between the geometry of a non-eccentric joint and eccentric joint is represented in Figures 4.5.a and 4.5.b, respectively. Model III (Figure 4.4.c) is similar to model II but with the inclusion of springs to represent the splice connection used in the bottom chord of the truss. The locations of the splice joints are shown in Fig 4.4.c with an "x" mark. The two sides of the timber members at the splice locations were connected with a torsional spring. The stiffness of these springs

was arbitrarily selected to be small in comparison with the axial stiffness of the bottom chord members. In addition, both sides of these members were constraint to translate together (Section 4.4).

As was also noticed in the field, each arch was composed of several simple elements that span between the vertical members. The members composing the arch are connected to the truss vertical members using two steel bolts. Therefore, it was necessary to break the continuity of the arch at these locations in model IV (Figure 4.4.d). This was accomplished by inserting a rotational spring with a small stiffness coefficient at each end of the element which is indicated with an open circle on Figure 4.4.d. Furthermore, the ends of each arch member were constrained to follow the movement of the vertical member at the intersection location. The connections between the diagonal and the vertical posts were modeled utilizing a similar approach. Model V (Figure 4.4.e) is similar to model IV but the moments at the ends of the diagonal members were released. Model VI (Figure 4.4.f) is a replication of model V with the exception of releasing the moments at the end of the vertical member near its intersection with the bottom chord of the truss. Finally, model VII (Figure 4.4.g) is similar to model VI but the modeling was done in accordance with the constructed top chord of the truss members. Examination of the in service Burr arch bridge indicated that the top chord member was constructed as simple members in the first and last panels of the truss, while as continuous members over the two of the interior panels on each side of the truss center vertical. Therefore it was necessary to model the top chord members as shown in Figure 4.4.g, i.e., releasing the moments at the ends of each member where such a discontinuity occurs.

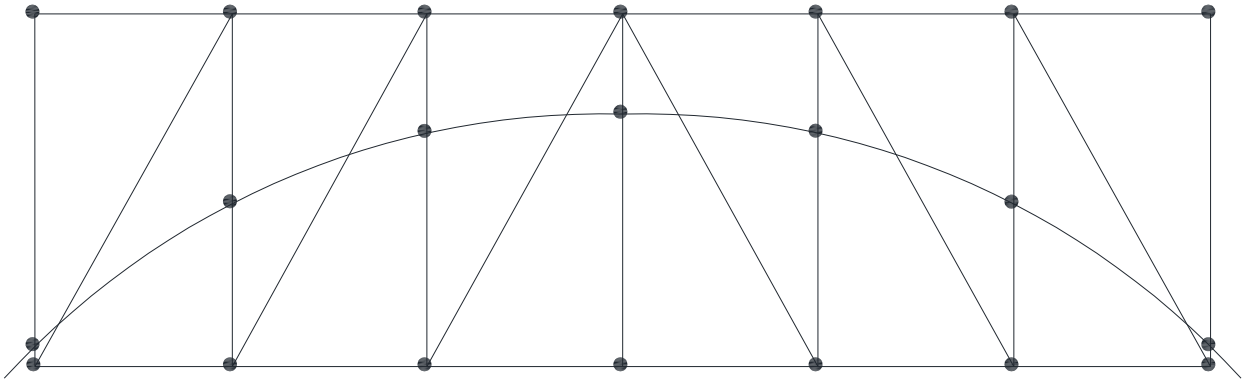

a: Model I

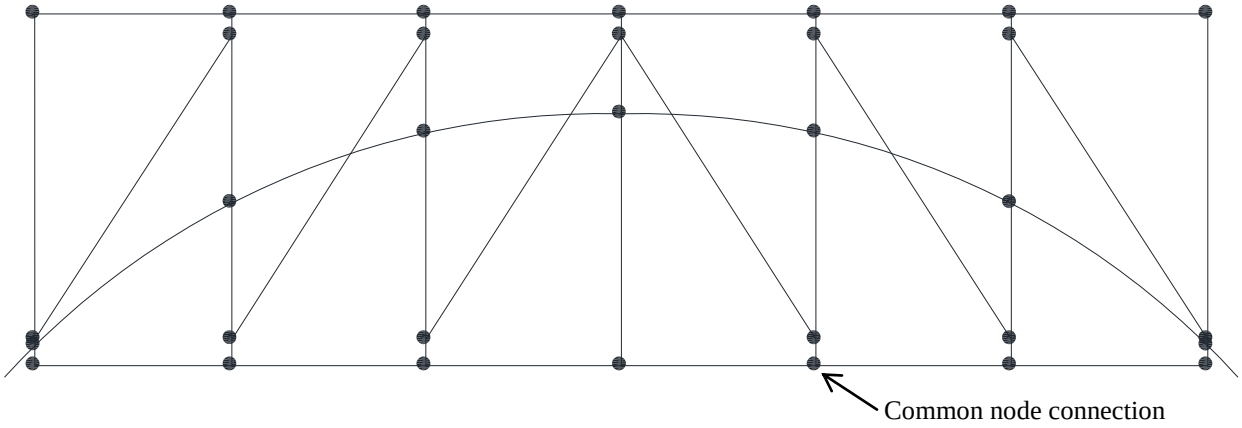

b: Model II

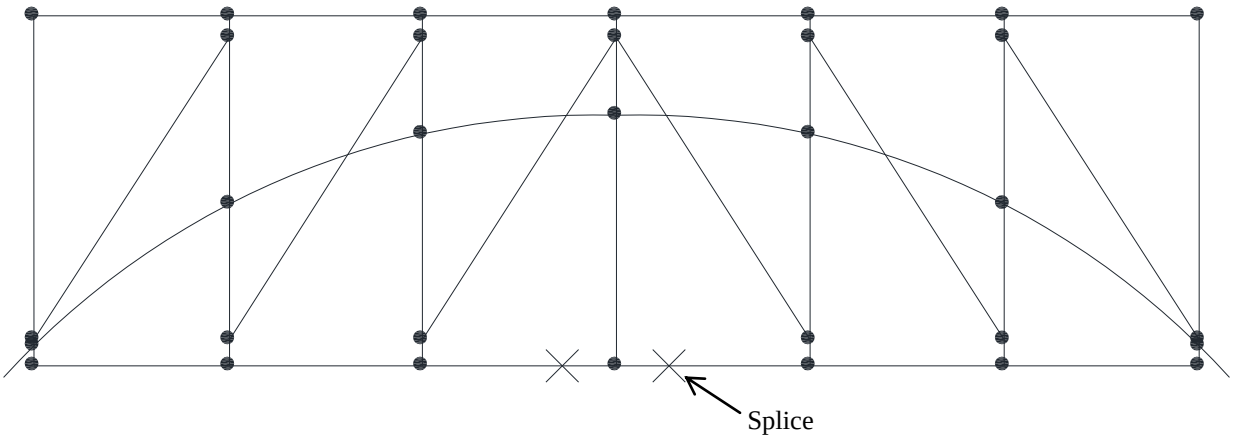

c: Model III

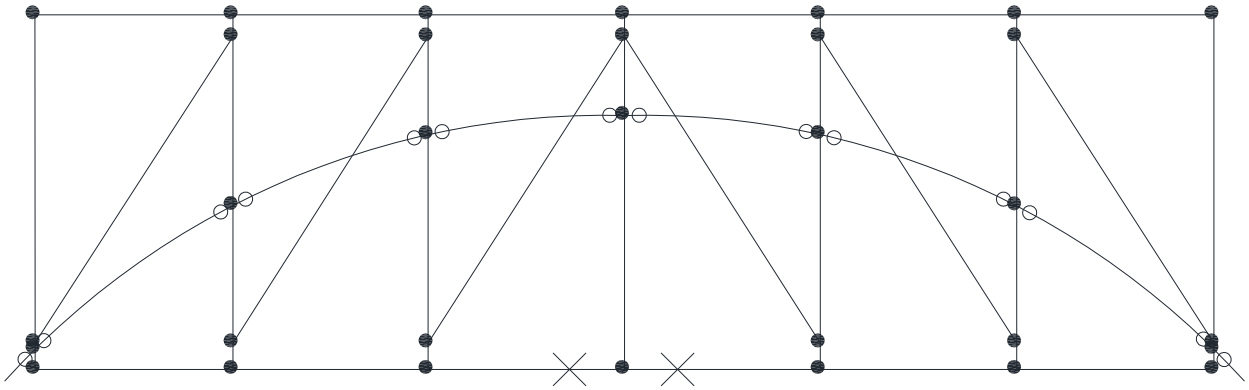

d: Model IV

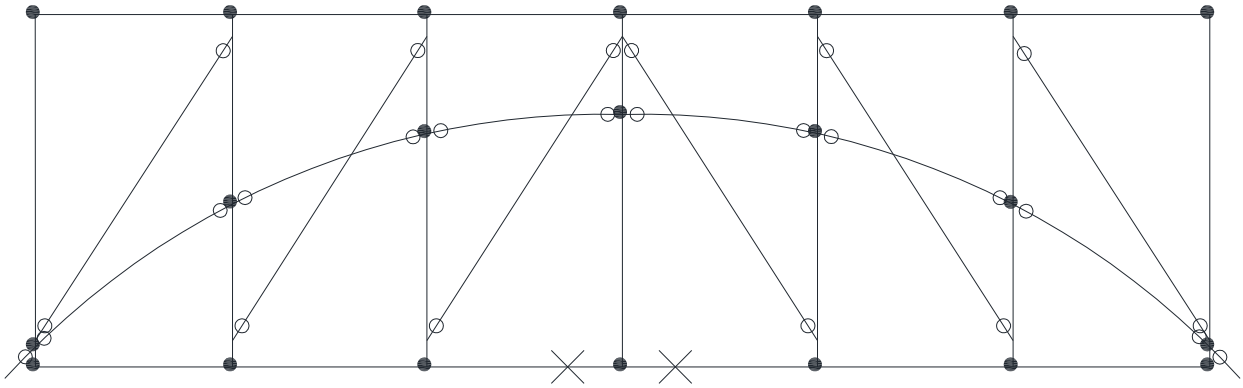

e: Model V

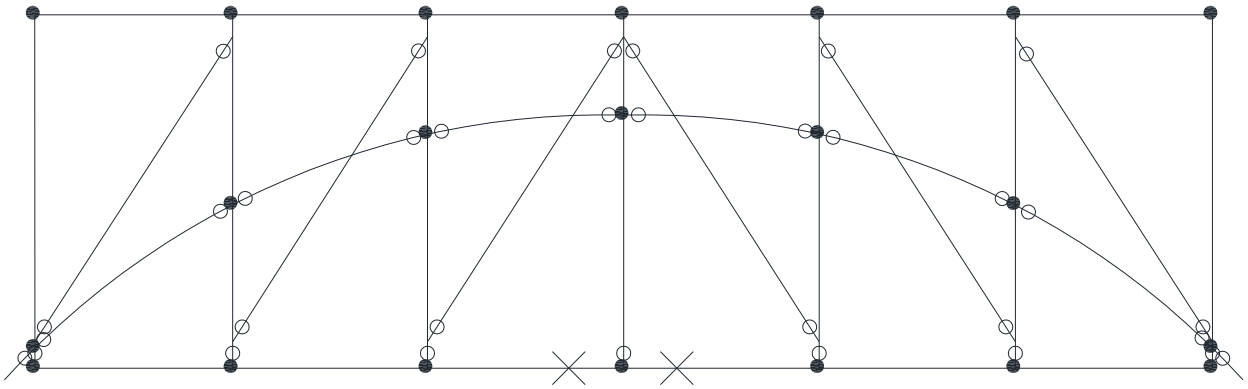

f: Model VI

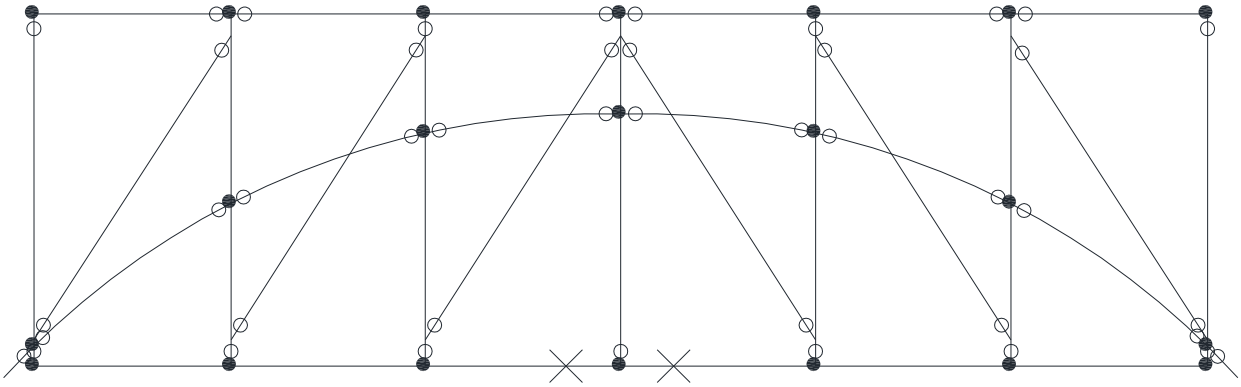

g: Model VII

Figure 4.4: Two dimensional stick model idealizations for the Zacke Cox Bridge

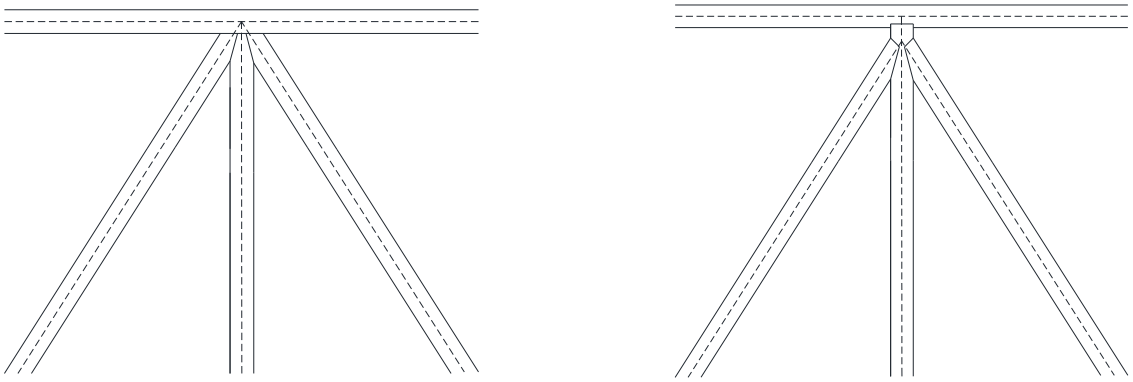

a. Non-eccentric joint (model I) b. Eccentric joint (model II)

Figure 4.5: Joint geometry representation of model I and II

4.5.1.2 Three Dimensional Modeling

The ANSYS three dimensional stick models of the Burr arch main supporting element are shown in Figures 4.6.a and 4.6.b (models VIII and IX, respectively). These models utilize a similar idealization of that used in model VII shown in Figure 4.5.g. In addition to that, three dimensional beam elements were used to represent the bolted connections that existed in the modeled portion of the bridge structure. In model IX, the arch structure was eliminated from the finite element. This was done to investigate the contribution of the arch in the deformation of the modeled Burr arch bridge. The portion of the applied load that was transmitted to each main supporting element was equally divided between the two members of the truss bottom chord as shown in Figure 4.6.

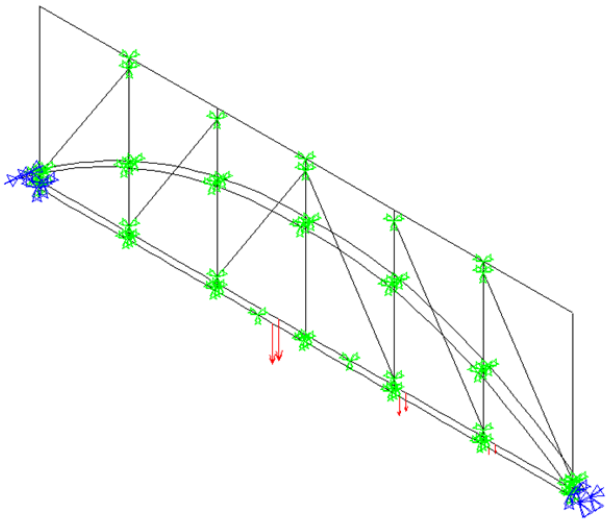

a: Model VIII

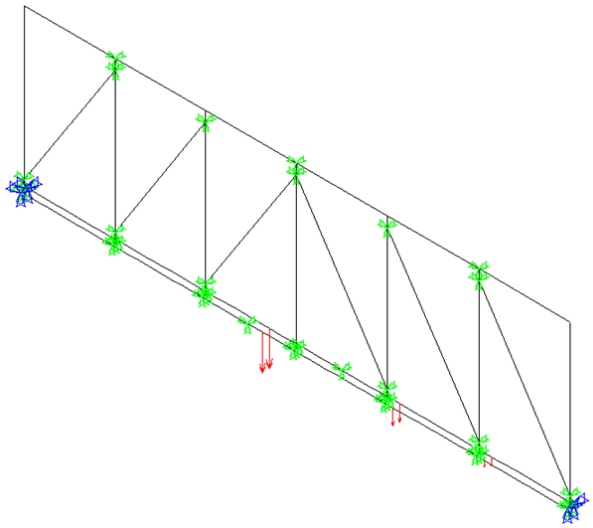

b: Model IX

Figure 4.6: Three dimensional stick model idealizations for the Zacke Cox Bridge

4.5.2 Boundary Conditions

With respect to the boundary conditions, both the arch and truss components were evaluated. By visual inspection in the field, the bridge truss structure was assumed to be simply supported while the arch portion of the bridge structure was supported at each end with an inclined support. For the finite element model purposes, the west end (left) of the

truss was modeled as a pinned support, while the other end was modeled as a roller support. Due to the construction of the arch at the bearing end locations, both ends of the arch were modeled as roller supports that where orientated so that the reaction forces at these supports were acting in the tangential direction to the arch member. Lastly, at each bearing condition, the truss and arch were restrained from moving in the direction perpendicular to the structure. The above discussion boundary condition idealization may be referenced below in Figure 4.7.

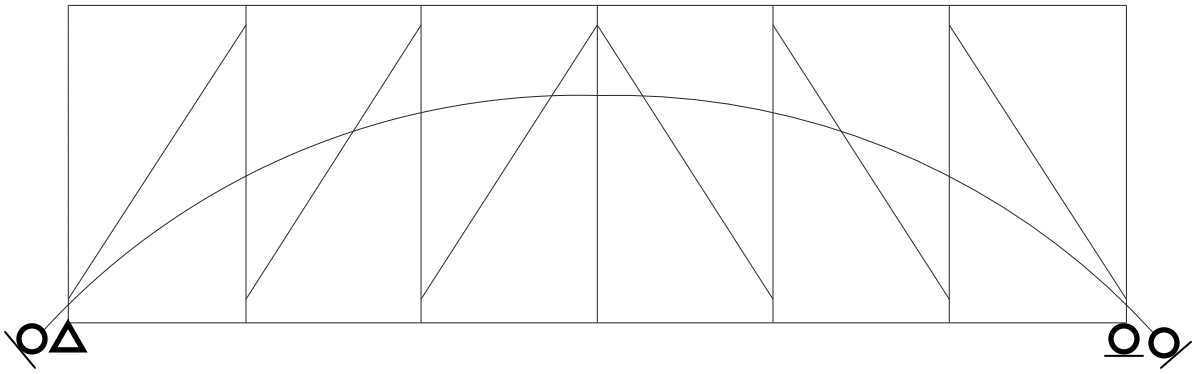

Figure 4.7: Boundary conditions for the Zacke Cox Bridge

4.5.3 Bridge Loading

To be able to compare the field and finite element results, the location of the truck that would create a large displacement within the bridge was selected. This loading case occurred when the heaviest axle, i.e., the back axle, was placed at the location of a floor beam just left of the center vertical member. This configuration of the back axles forces the front axle of the small truck to be placed between two vertical members and not directly above a floor beam. To determine the front axle load distribution to the two nearest floor beams on either side of the front axle load, basic statics was utilized. Figure 4.8.a represents the actual location of the back and front axles of the small test truck during field testing while Figure 4.8.b represents the idealized truck axle load distribution to the floor beams utilized in the finite element stick models. The same assumption and axle load distribution approach was utilized for the large test truck. Figure 4.9 illustrates the position of the large truck axles and the locations where the axle loads were applied in the finite element stick models.

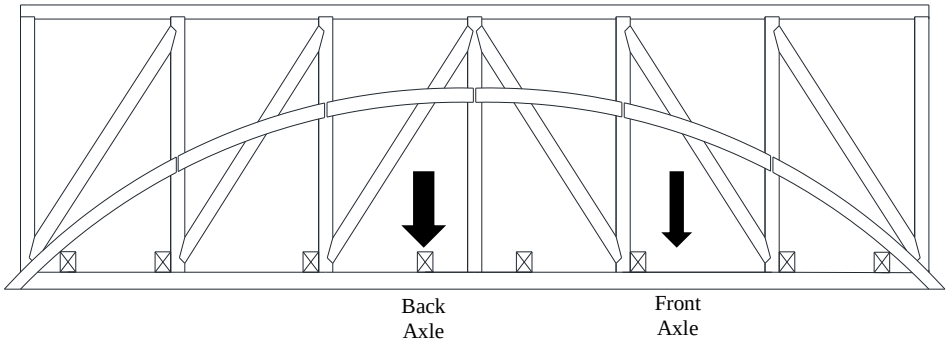

a: Actual field truck loading position

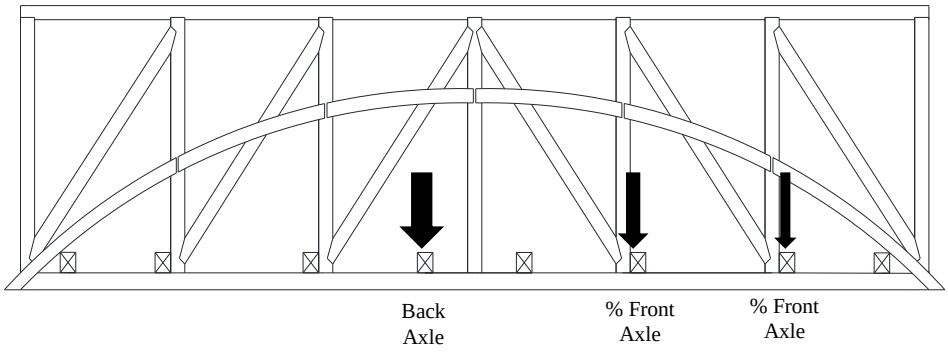

b: Analytical representation of the truck loading distribution

Figure 4.8: Elevation view of Zacke Cox Bridge representing the small test vehicle's loading assumptions

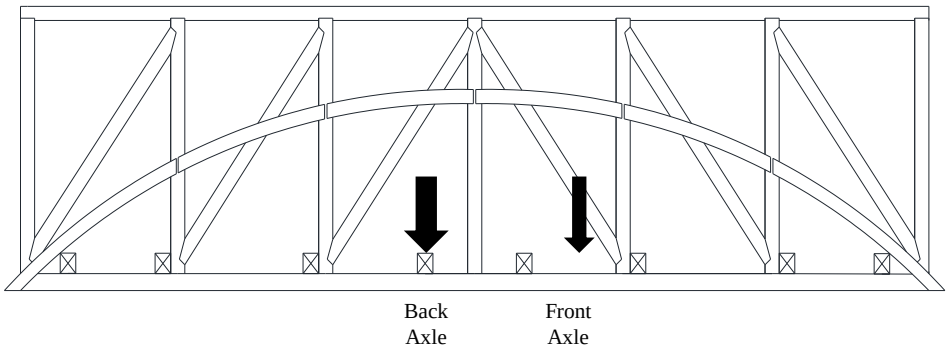

a: Actual field truck loading position

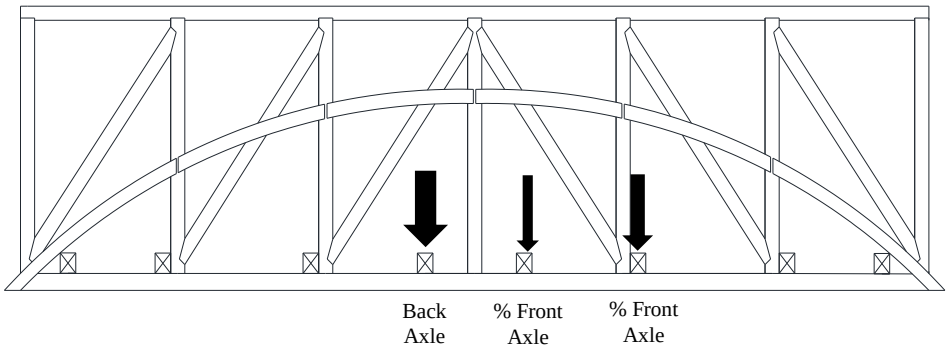

b: Analytical representation of the truck loading distribution

Figure 4.9: Elevation view of Zacke Cox Bridge representing the large test vehicle's loading assumptions

4.6 Portland Mills Bridge

4.6.1 Finite Element Model

The finite element idealization employed in model VIII was used to construct the finite element stick model for the Portland Mills Bridge. A three dimensional stick model was developed that represented the construction details found within the bridge structure. The double bottom chord was modeled as is present in-situ. The double concentric arch was modeled such that on each side of the truss, the double arch members were modeled as one monolithic timber member instead of two timbers present in-situ. Just as was completed in the Zacke Cox Bridge model VIII, the Portland Mills Bridge model broke the continuity between the timber member connections, i.e. between the diagonals and verticals, arch and verticals, and top chord and verticals, by releasing the moment at the end of each member. Then at these locations, a rotational spring with a small stiffness coefficient in relation to the bottom chord member's axial stiffness was inserted. This idealization is indicated by an open circle on Figure 4.10. Also, rotational springs were utilized at the locations of the splice joints both in the bottom and top chords, represented with an "x" in Figure 4.10. As previously done in model VIII, three dimensional elements were used to represent the bolted connections within the bridge; the bottom chord members and vertical and the arches and vertical. Lastly, due to the modeling generalization of the double concentric arch, each arch

ring was idealized as a simple member between each of the truss which differs from the construction detail. Figure 4.11, illustrates the continuity of the top and bottom arches where the arch rings alternate discontinuity at each vertical. The three dimensional analytical model may be seen in Figure 4.12.

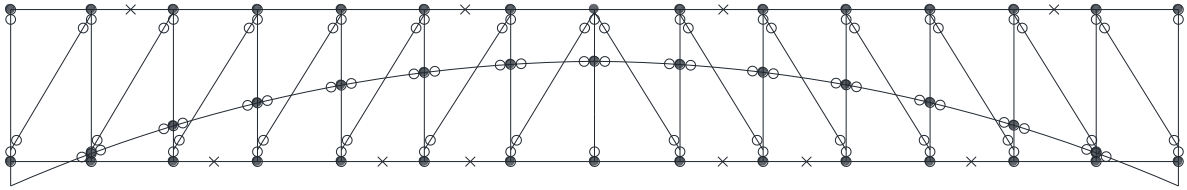

Figure 4.10: Analytical stick model idealization for Portland Mills Bridge

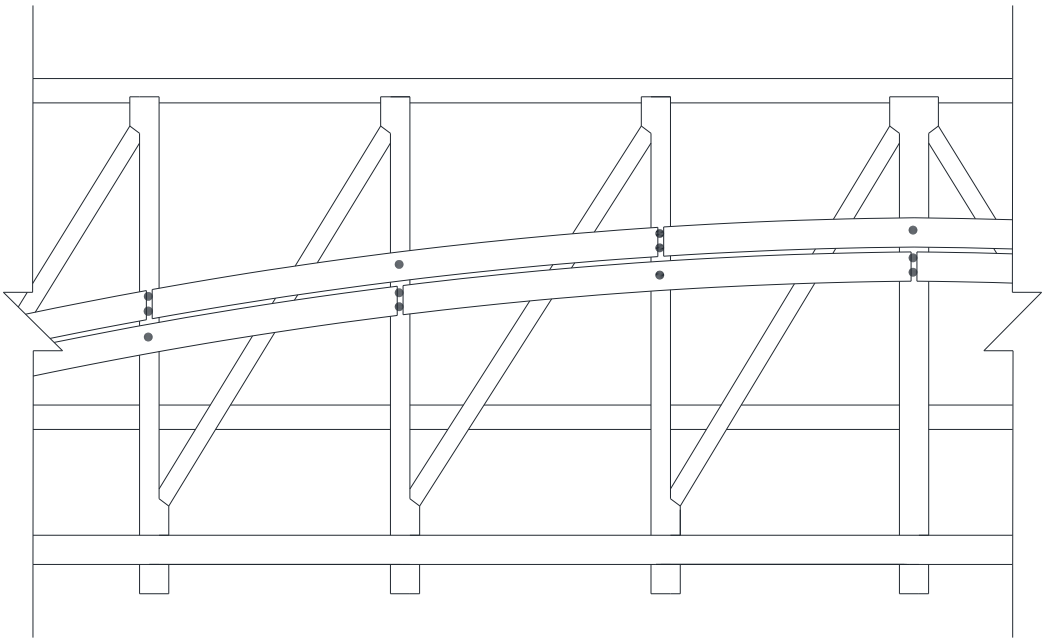

Figure 4.11: Detailed view of double concentric arch construction details

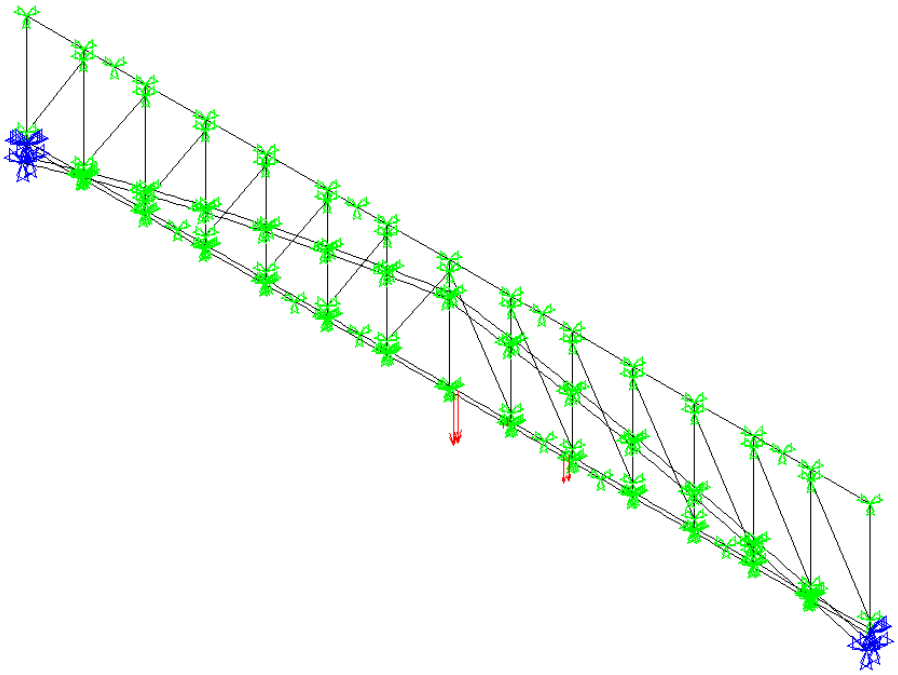

Figure 4.12: Three dimensional stick model for the Portland Mills Bridge

4.6.2 Boundary Conditions

With visual inspection in the field, the research team concluded that the boundary conditions for the Portland Mills Bridge were exactly the same as to those in the Zacke Cox Bridge for the finite element stick model. The east end (left) of the truss is pinned and the other end is roller supported. Both ends of the arch had a roller supported orientated in such a way that the reaction forces of the supper acted in a tangential direction to the arch member. Lastly, all four bearing locations were restrained from moving in the direction perpendicular to the structure.

4.6.3 Bridge Loading

As discussed previously, the Portland Mills Bridge was only load tested with the small truck. The location for application and quantity distribution of the axle loads within the finite element stick model was completed in a similar fashion as was done for the Zacke Cox Bridge. Figure 4.13 shows both the location of the test truck's axle location in the field and axle load distribution to the relevant floor beams within the analytical model.

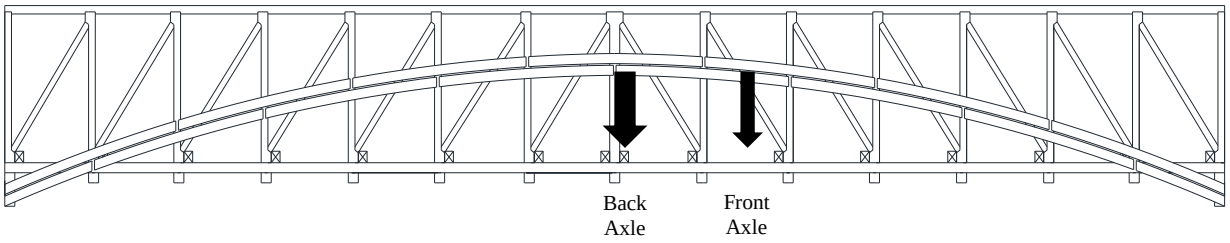

a. Actual field truck loading position

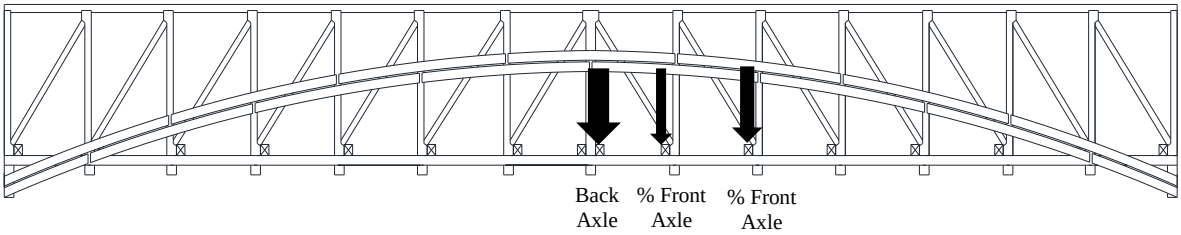

b. Analytical representation of the truck loading distribution

Figure 4.13: Elevation view of Portland Mills Bridge representing the small test vehicle's loading assumptions

4.7 Cox Ford Bridge

4.7.1 Finite Element Model

The finite element stick model assumptions for the Cox Ford Bridge were identical to those made for the Portland Mills Bridge except for the location of the splice joints in the bottom chord. Figures 4.14 and 4.15 illustrate the analytical modeling assumptions utilized.

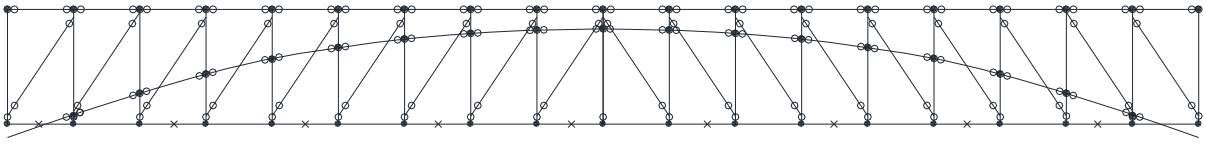

Figure 4.14: Analytical stick model idealization for the Cox Ford Bridge

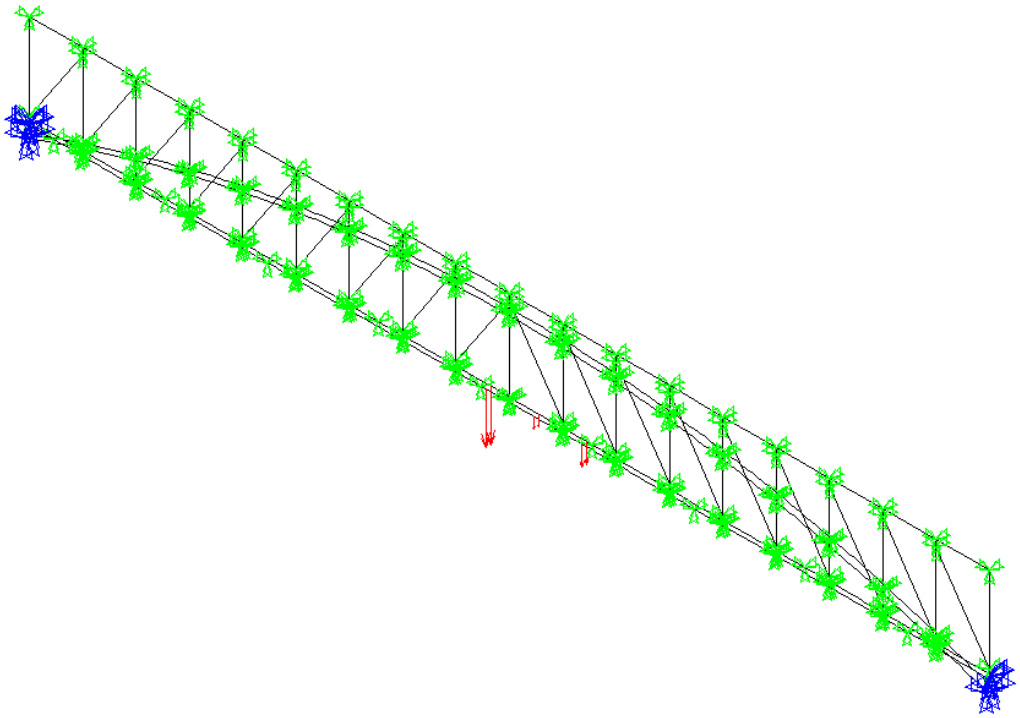

Figure 4.15: Three dimensional stick model for the Cox Ford Bridge

4.7.2 Boundary Conditions

Unlike the Zacke Cox and Portland Mills Bridges, from visual field inspection the Cox Ford Bridge has different boundary conditions for the arch. Similar to the other two bridges discussed previously, the south end (left) of the truss was pinned supported while the other end was roller supported. But the arch was assumed to be pinned supported at both ends. Also, due to the three dimensional analysis, all of the bearing conditions were restrained from movement in the direction perpendicular to the structure.

4.7.3 Bridge Loading

The test truck loading locations and quantities were determined similarly to what was done in the Zacke Cox Bridge and Portland Mills Bridge. Both test vehicles, the small and large, were able to be utilized in testing this structure. Figures 4.16 and 4.17 represent the axle locations in the field and the analytical representation for both the small and large test trucks, respectively.

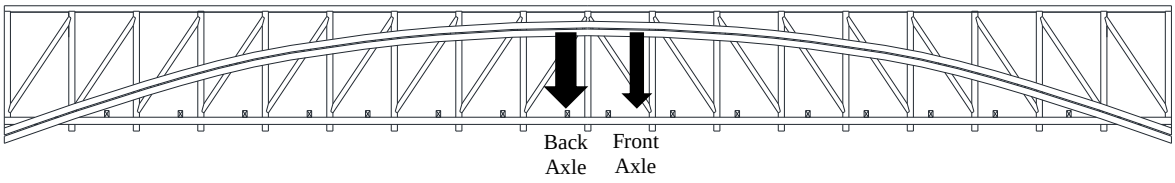

a. Actual field truck loading

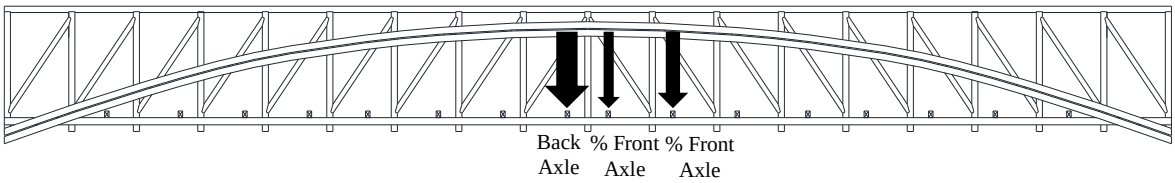

b. Analytical representation of the truck loading distribution

Figure 4.16: Elevation view of Cox Ford Bridge representing the small test vehicle's loading assumptions

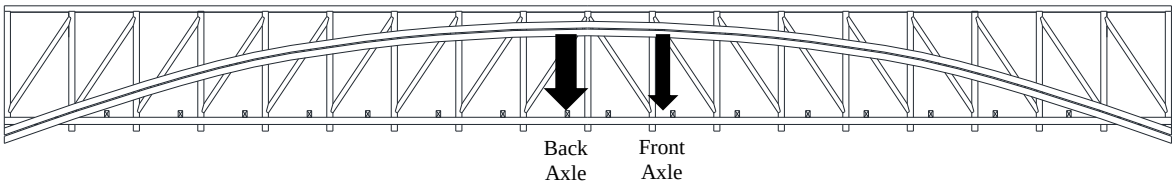

a. Actual field truck loading

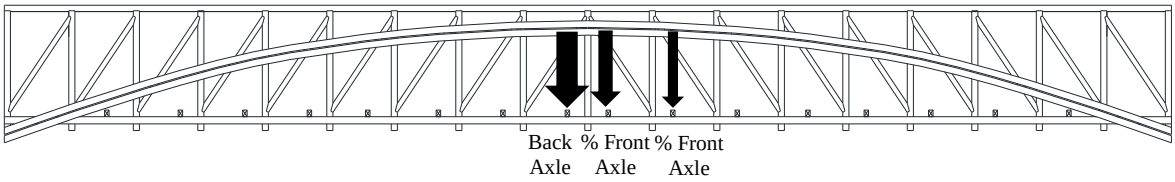

b. Analytical representation of the truck loading distribution

Figure 4.17: Elevation view of Cox Ford Bridge representing the large test vehicle's loading assumptions

4.8 Material Properties

The material properties such as the modulus of elasticity, E, and poisson's ratio, υ, were determined from the Wood Engineering Handbook (Second Edition) along with guidance provided by the FPL engineers. With this guidance, the timber within the structure was assumed to be dry Eastern Hemlock. For the bolts present in the structure, the typical property values of steel were utilized. The material property values used for both the timber

members and steel bolts are represented in Table 4.3. Lastly, from evaluation of the axial stiffness of a typical timber member, an appropriate arbitrary small spring stiffness, k, was selected to be 10,000 in/in.

Table 4.3: Material properties for analytical modeling

Material	Modulus of Elasticity (psi)	Poisson's Ratio
Timber	1,200,000	0.3
Bolts	29,000,000	0.3

CHAPTER 5: RESULTS AND DISCUSSION

The measured deflection and strain results from the field tests of the Zacke Cox, Portland Mills and Cox Ford bridges in Indiana were used to validate of the results obtained from the analytical models. Due to the slight differences in geometric properties, the results for each of the three bridges will be discussed individually with the findings resulting in one overall recommendation that can be utilized by bridge engineers in developing analytical models and rating similar types of these historical timber covered bridges.

5.1 Zacke Cox Bridge

5.1.1 Deflection Results at the Mid-Span and Quarter-Span Points

As previously mentioned, the Zacke Cox Bridge was tested using two different trucks. Deflections in the field were recorded at the mid and quarter-span points for each of the two main supporting elements.

Figure 5.1 shows the measured deflection plots for the quarter and mid-span points for the north main supporting truss as a function of the truck's front axle location on the bridge. The recorded field test data showed a downward deflection of 0.052 in. and 0.016 in. that occurred at the mid-span and quarter-span points, respectively, when the north truss was loaded with the small truck (See section 4.5.3 for truck loading). When the bridge was loaded with the large truck downward deflections of 0.189 in. and 0.062 in. were recorded at the mid and quarter-span points, respectively. These recorded deflections were used to validate the results that were obtained when analyzing the different analytical models shown in Figure 4.4. Tables 5.1 and 5.2 summarize the results obtained from the analytical modeling and the field test deflections for the loading of the small and large truck, respectively.

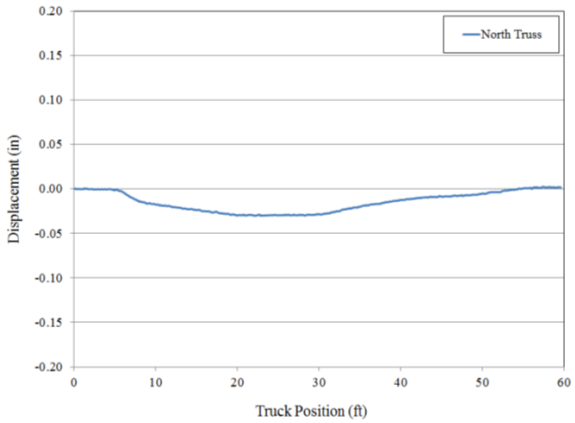

a. Quarter-span deflection – small truck

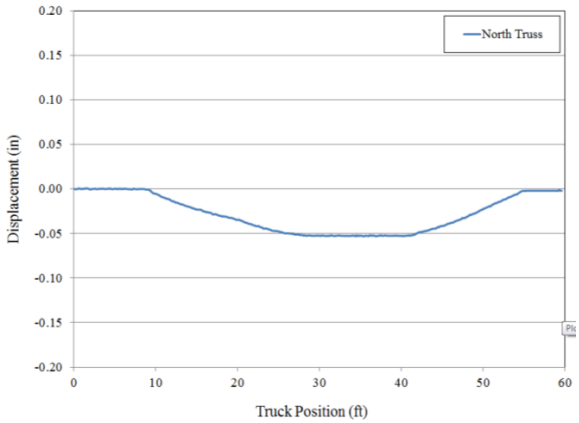

b. Mid-span deflection – small truck

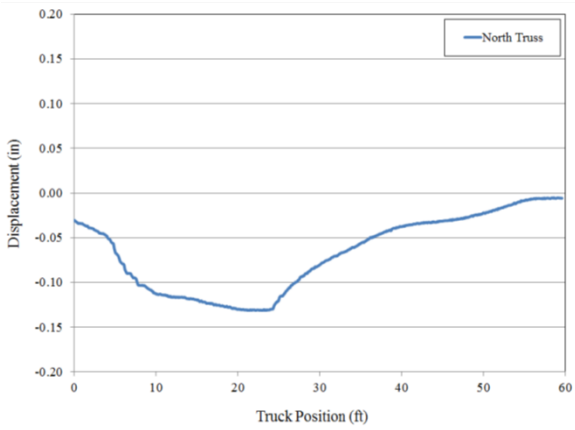

c. Quarter-span deflection – large truck

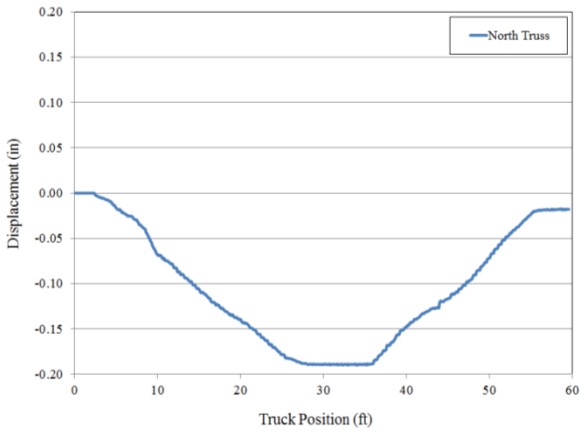

d. Mid-span deflection – large truck

Figure 5.1: Deflection results for the Zacke Cox Bridge as a function of the load truck position on the bridge (run down the centerline of the bridge) – small and large truck

Table 5.1: Analytical deflection results for the Zacke Cox Bridge – small truck

Model Number	Mid-span Deflection (in.)		Quarter-span Deflection (in.)	
	Analytical	Field	Analytical	Field
Model I	0.032	0.052	0.012	0.016
Model II	0.030	0.052	0.012	0.016
Model III	0.034	0.052	0.013	0.016
Model IV	0.035	0.052	0.013	0.016
Model V	0.035	0.052	0.013	0.016
Model VI	0.039	0.052	0.011	0.016
Model VII	0.043	0.052	0.013	0.016
Model VIII	0.041	0.052	0.006	0.016
Model IX	0.076	0.052	0.031	0.016

From Table 5.1, one may notice that modeling the main supporting element of the bridge and ignoring the construction details of the joints resulted in a smaller deflection than those obtained from the field tests. On the other hand, the results summarized in Table 5.1 showed that utilizing the finite element idealization in models I through VI in calculating the mid-span deflection yielded results that are not comparable to those obtained from the field test. One potential factor affecting the differences in the analytical and field test data is the use of the published timber material Young's modulus in the analysis. This published value may significantly vary from the actual material properties of the timber within the bridge to result in the observed differences (Section 5.4.3). Table 5.1 also suggests that the arch does contribute to the load carrying capacity of the bridge's structure to some degree. For example, excluding the arch from the finite element model (model IX) resulted in a deflection of 0.076 in. at the bridge mid-span. This is about 42.5%, 45.2% and 30.7% larger than the deflection obtained from model VII, model VIII and the field measured values, respectively.

Even with the mid-span deflection of model VII closely representing the field data, the three dimensional stick model, model VIII, was developed to best represent the geometry and load distribution of the two bottom chord members of the truss. As can be seen in Table 5.1, there was a slight decrease in the deflection obtained using model VIII when compared to the deflection that was calculated using the two dimensional stick model (model VII). However, the author of this report concluded that model VIII is the most appropriate idealization to be utilized hereafter for analyzing the other two bridges. This was due to the fact that this three dimensional stick model idealization allows a user to include the splice joints at its exact locations as used in both of the bottom chord elements of the truss.

Table 5.2 summarizes the deflection results when the bridge was subjected to the large truck load shown in Table 3.4. As can be noticed, the ratio of the large to the small truck is about 1.8. Hence, one may expect the deflection under the large truck to be 1.8 times larger than that caused by the small truck load. However, one must also notice the difference between the axle loads of both trucks could easily have some effect on the measured and calculated deflections. The effect of these differences was noticed from both analytical and measured deflections. Table 5.2 illustrates that the deflection due to the large truck is

approximately 1.92 times the deflection obtained when the bridge was loaded with the small truck. On the contrary, the field test results showed that under the large truck, the measured deflection was about 3.63 times that was caused by the small truck. This discrepancy could be due to the fact that the bridge structure in the field does not behave elastically. Another reason for this difference could be due to an inaccuracy of the measured deflections that were caused by the technique used to mount the apparatuses that were used to measure the deflections.

Table 5.2: Analytical deflection results for the Zacke Cox Bridge – large truck

Model Number	Mid-span Deflection (in.)		Quarter-span Deflection (in.)	
	Analytical	Field	Analytical	Field
Model VIII	0.079	0.189	0.016	0.062

5.1.2 Deflection in the Vicinity of the Splice Joint

Figures 5.2 and 5.3 illustrated the localized effects of the splice joints. The splice joint left of mid-span (Figure 3.6) demonstrates the local behavior of the joint within the bottom chord due to the relatively close loading conditions. As can be noticed, the discontinuity of one member of the two bottom chord members at the joint location experiences a larger deflection than the other adjacent continuous member. In addition, it was noticed that the portion of the discontinuous bottom chord member left of the joint location experiences an upward deflection. From this finding, one would expect that the two members forming the bottom chord of the truss to be subjected to different strains that are different in magnitude and directions. For example near the location of the splice, the top and bottom faces of the discontinuous member will be in tension and compression, respectively. Opposite directions of the strains will be expected in the top and bottom faces of the continuous member of the bottom chord. The calculated and measured strain results are documented in Section 5.1.3.

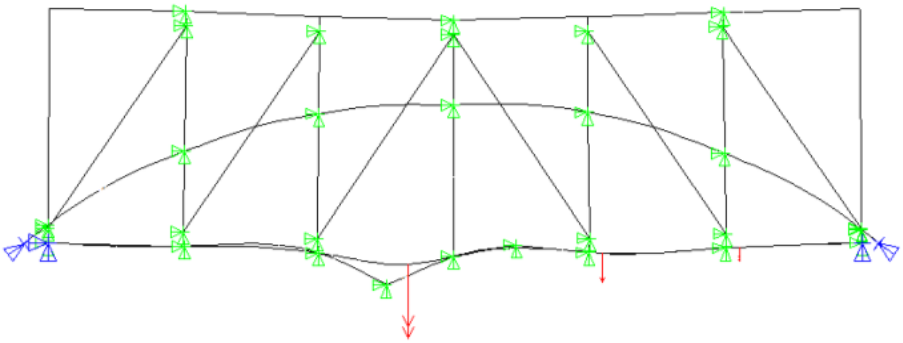

Figure 5.2: Elevation view of the analytical deflected shape of model VIII for the Zacke Cox Bridge

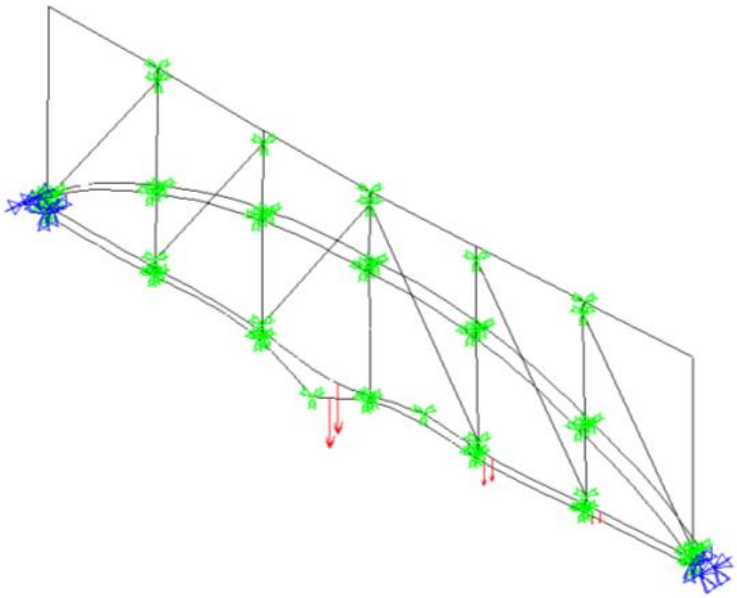

Figure 5.3: Analytical deflected shape of model VIII for the Zacke Cox Bridge

5.1.3 Strain Results

The strain values from the field results were compared with the analytically determined strain values at the same specific locations. The locations of the strain gauges that were placed on different elements of the north and south main supporting elements are illustrated in Figure 5.4. Table 5.3 lists the measured and calculated results that were obtained using model VIII.

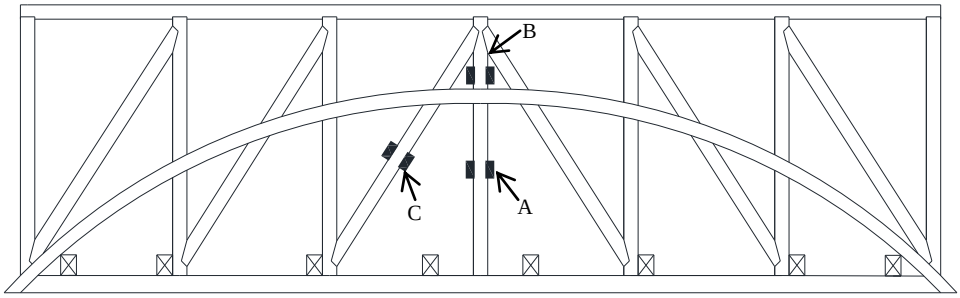

a. North truss

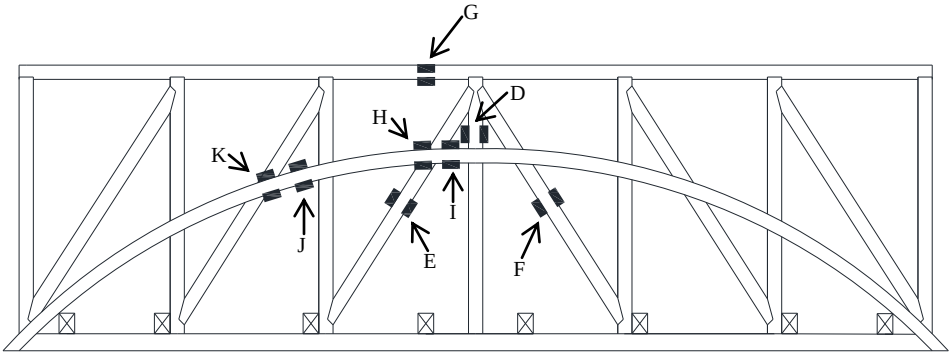

b. South truss

Figure 5.4: Strain gauge truss locations for the Zacke Cox Bridge

Table 5.3: Field and analytical strain results for the Zacke Cox Bridge – large truck

Model VIII	Strain Gauge Location	Member Description	Field testing top* (μ strain)	ANSYS top* (μ strain)	Field testing bottom (μ strain)	ANSYS bottom (μ strain)
North Truss	A	Vertical 4	30	64	19	52
	B	Vertical 4	28	46	10	53
	C	Diagonal	-24	-42	-12	-42
South Truss	D	Vertical 4	10	45	15	54
	E	Diagonal	-32	-42	-12	-42
	F	Diagonal	-2	-33	-18	-33
	G**	Top Chord	-10	-34	-38	-39
	H	Outward Arch	-30	-74	-43	-1
	I	Inward Arch	-45	-54	-20	-22
	J	Outward Arch	-39	3	-26	-79
	K	Inward Arch	-36	12	-29	-88
	L	Vertical 3	51	76	13	32

*Note: The top of the member is that of which is on the left when looking directly at the elevation view.
**Note: The top strain gauge was placed on the side face of the timber instead of the top face and the location on the side face was not documented.

Table 5.3 shows that the field and analytical strain values for specific timber members agree based on the direction of the strain value, i.e. positive as tension and negative as compression, but there is a discrepancy between the magnitudes. Potential sources of these discrepancies are discussed later within this chapter.

As mentioned in Chapter 3, the two bottom chord splice joints were each instrumented with six strain gauges (three on the top and three on the bottom). Gauge instrumentation for each of the splice joints is shown below in Figures 5.5 and 5.6. Table 5.4 compares the field data and analytical results for both of the splice joints instrumented below.

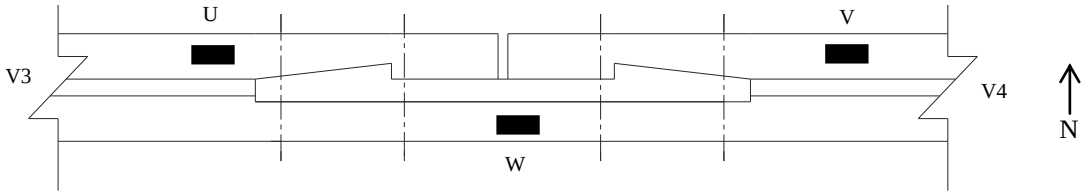

Figure 5.5: Plan view of bottom chord north truss joint with strain gauge locations for the Zacke Cox Bridge

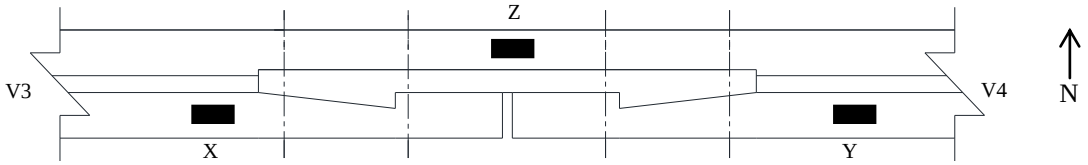

Figure 5.6: Plan view of bottom chord south truss joint with strain gauge locations for the Zacke Cox Bridge

Table 5.4: Field and analytical strain results for splice joints for the Zacke Cox Bridge – large truck

Model VIII	Strain Gauge Location	Field testing top* (μ strain)	ANSYS top* (μ strain)	Field testing bottom (μ strain)	ANSYS bottom (μ strain)
North Truss	U	43	217	0	-184
	V	55	130	-6	-98
	W	-63	-153	99	185
South Truss	X	32	217	-7	-184
	Y	8	130	2	-98
	Z	-39	-153	99	185

*Note: The top of the member is the top face of the bottom chord member when looking at the elevation view.

Examining Table 5.4 shows that the directions of the strains predicted by the analytical results agree with those observed in the field. However, there is a large difference in magnitude between the measured and calculated magnitude of these strains. Sources that could have potentially caused these discrepancies are discussed later within this chapter (Section 5.4).

5.2 Portland Mills Bridge

5.2.1 Deflection Results at the Mid-Span and Quarter-Span Points

As was previously discussed with the Zacke Cox Bridge, the Portland Mills Bridge was also load tested and the deflections were recorded at the mid and quarter-span points for each of the two main supporting elements. Figure 5.7 shows plots for the measured deflections at these locations for the south main supporting element as a function of the truck's front axle location. Downward deflections of 0.073 in. and 0.056 in. were recorded at the mid-span and quarter-span points, respectively. These field recorded deflections were used to validate the results of the analytical model. Table 5.5 lists the deflections at mid and quarter-span for the measured and calculated values.

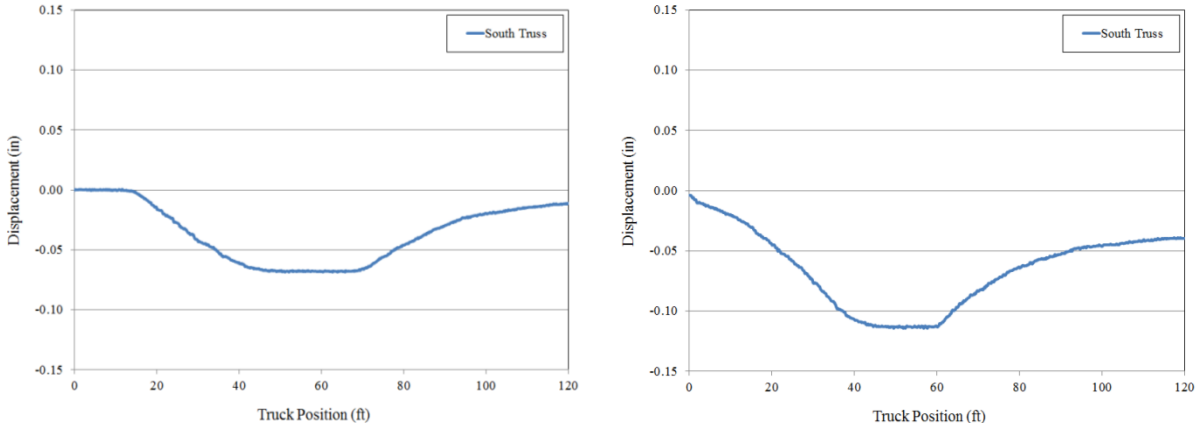

a. Quarter-span deflection – small truck

b. Mid-span deflection – small truck

Figure 5.7: Deflection results for the Portland Mills Bridge as a function of the load truck position on the bridge (run down the centerline of the bridge) – small truck

Table 5.5: Analytical deflection results for the Portland Mills Bridge – small truck

Model Number	Mid-span Deflection (in.)		Quarter-span Deflection (in.)	
	Analytical	Field	Analytical	Field
Portland Mills	0.082	0.073	0.031	0.056

Table 5.5 shows that there are discrepancies between the measured and calculated deflections. The sources of these discrepancies are discussed later within this chapter.

5.2.2 Deflection in the Vicinity of the Splice Joint

Further evaluation of the analytical model's deflected shape (Figures 5.8, 5.9 and 5.10) showed that many of the same characteristics within the splice joint regions were found for the Portland Mills Bridges as was within the Zacke Cox Bridge. Within Figure 5.10, the localized behaviors of two consecutive splice joints within the bottom chord are seen in region "A" and "B". As can be seen within area "A", the discontinuous bottom chord member has a greater downward deflection than that of the adjacent continuous bottom chord member. While in area "B", what was the continuous member in "A" becomes the discontinuous member in "B" which has a downward deflection greater than the continuous member. This was to be expected due to the modeling of the discontinuity at the location of the splice joint in each bottom chord member. From this localized behavior, there is an expectation that within the strain values that the discontinuous members at a specific location will have a tension value on the top face and compression on the bottom face for the bottom chord member. While the continuous bottom chord member will experience the exact opposite behavior. While for the top chord splice joint, region "C" in Figure 5.10, there is an expectation for slight deflection movement; potentially upwards from the field data.

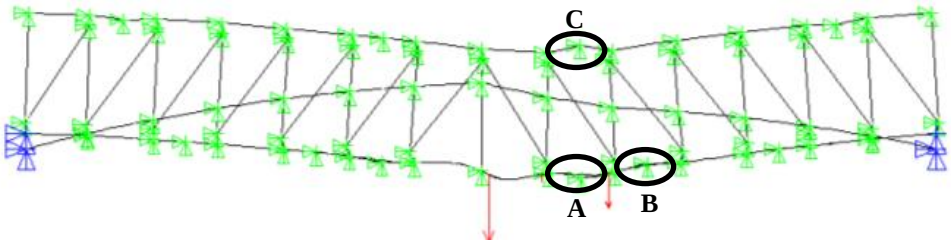

Figure 5.8: Elevation view of the analytical deflected shape for the Portland Mills Bridge

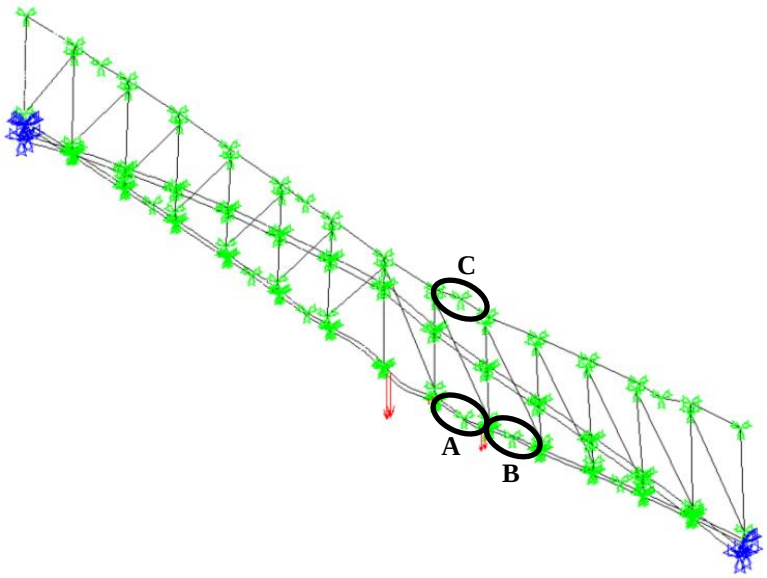

Figure 5.9: Analytical deflected shape for the Portland Mills Bridge

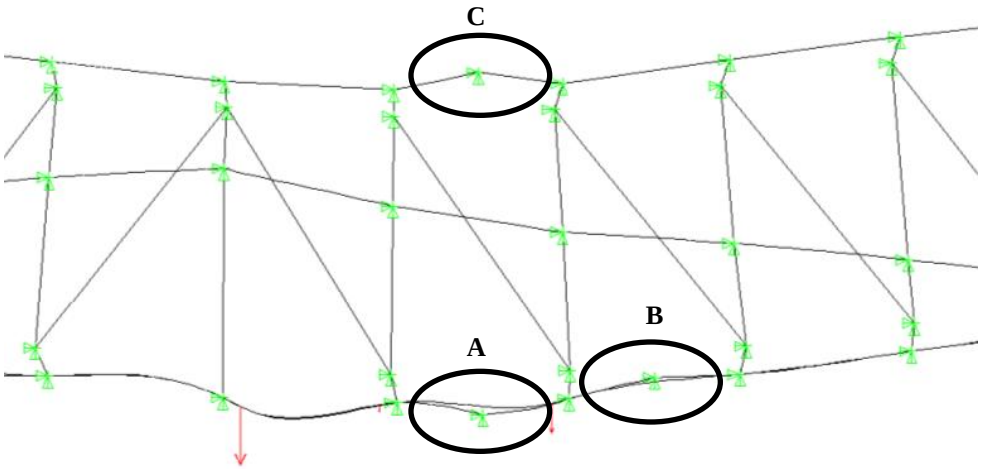

Figure 5.10: Close up elevation view of the deflected shape between verticals 7 to 12

5.2.3 Strain Results

The recorded strain values from the field at the different locations were compared with the analytically determined values. The locations that were evaluated on the truss are referenced in Figure 5.11. Table 5.6 lists both the field and analytical values for the Portland Mills Bridge.

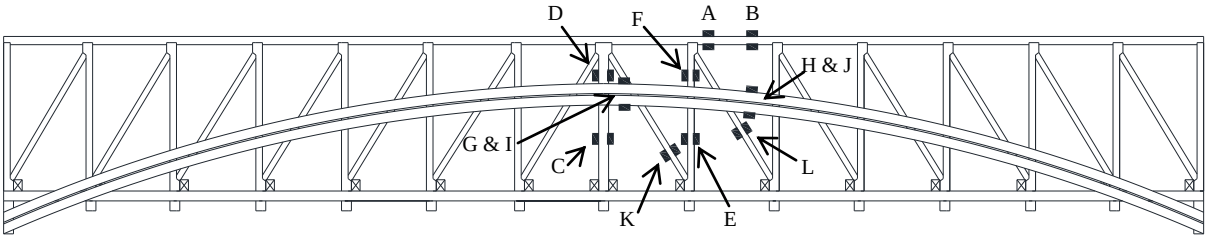

Figure 5.11: Strain gauge truss locations for the Portland Mills Bridge

Table 5.6: Field and analytical strain results for Portland Mills Bridge – small truck

	Strain Gauge Location	Member Description	Field testing top (μ strain)	ANSYS top (μ strain)	Field testing bottom (μ strain)	ANSYS bottom (μ strain)
South Truss	A	Top Chord – near Vertical 9	-37	-35	-5	-26
	B	Top Chord – near Vertical 10	-19	-31	-21	-30
	C	Vertical 8 – bottom	15	33	6	18
	D	Vertical 8 - top	23	-16	3	27
	E	Vertical 9 – bottom	9	7	12	-1
	F	Vertical 9 – top	9	3	8	2
	G	Arch – outward near Vertical 8	-19	-25	7	-23
	H	Arch – outward near Vertical 10	-25	-22	-12	-25
	I	Arch – inward near Vertical 8	-26	-25	1	-23
	J	Arch – inward near Vertical 10	-16	-22	-9	-25
	K	Diagonal – 8 and 9	0	11	1	11
	L	Diagonal – 9 and 10	-9	-4	-5	-4

*Note: The top of the member is that of which is on the left when looking directly at the elevation view.

As can be noticed from Table 5.6 the measured and calculated strains are in agreement in the direction but with some differences in magnitude. These differences can be explained with the same reasons as discussed in Sec. 5.1. One interesting finding is that both field and analytical results showed that the direction and the magnitude of the strain in the diagonal members labeled "K" and "L" are is in tension and compression, respectively. This is unlike what was observed in the Zacke Cox Bridge where the diagonals on both sides of

mid-span were determined to be in compression. Applying basic structures theory, without the presence of the arch and for a symmetrical truss and in the case here, one would expect that all the diagonal members to experience compression forces and strains. The change in the sign of the strains in the diagonals labeled "K" and "L" in Figure 5.11 of the Portland Mills Bridge could be contributed to the arch in how the loads are transferred in this large span bridge structure.

Strain gauges were utilized within the bottom chord to evaluate the strain values and characteristics of the stop-splayed splice joint. The locations which were considered in the field are located in Figure 5.12. Table 5.7 summaries the values of both the field and analytical strain values and magnitudes.

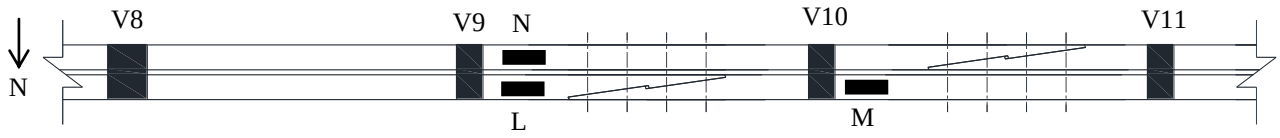

Figure 5.12: Plan view of bottom chord joint with strain gauge locations on the south truss

Table. 5.7: Field and analytical results for splice joint for the Portland Mills Bridge – small truck

	Strain Gauge Location	Field testing top (μ strain)	ANSYS top (μ strain)	Field testing bottom (μ strain)	ANSYS bottom (μ strain)
South Truss	L	1	35	-1	-21
	M	-6	14	0	-21
	N	1	25	3	-11

*Note: The top of the member is the top face of the bottom chord member when looking at the elevation view.

As can be seen in Table 5.7, there is no distinct characterization for the behavior of the bottom chord splice joint for both the field and analytical results. This could potentially be contributed to not comparing the strains at the exact locations of the instrumentation or due to the effect of the behavior of the splice joint between verticals 10 and 11 in the vicinity of the splice joint being evaluated between verticals 9 and 10.

5.3 Cox Ford Bridge

The Cox Ford Bridge followed a similar analytical evaluation process as was completed in the Zacke Cox and Portland Mills bridges. As discussed previously, this bridge has many more unknowns when compared to the other two bridges evaluated. Two of these unknowns, material properties and in-situ measurements, may have created additional discrepancies between the field and analytical results. However, this bridge was also analyzed and the comparison evaluation between the field and analytical values are listed in the Appendix. Upon further knowledge becoming available, the Cox Ford Bridge must be reanalyzed and compared with the field test results.

5.4 Discussion

From the study presented above, one may notice that there are discrepancies between the field test data and analytical results for both the deflection and strain results. These discrepancies may be the results of several factors. The following is a trial to explain the sources of these discrepancies.

5.4.1 Data Collection Method

Each of the Bridge Diagnostics Inc. strain gauges was attached to the timber members with two screws. Each screw was incrementally tightened until the strain gauge was level with the timber member from visual inspection. Across the surface of the timber where the strain gauge was mounted, the strain value could easily be affected by the orientation of the grains and the roughness of the timber. In addition, it is the opinion of this author, that the magnitude of the clamping force used to tighten the strain gauge to the timber could also affect the measured strain values.

Another reason for the discrepancy between the measured and calculated strains could be due to restrictions of accessibility to the top or bottom face of some timber members. In the field, some strain gauges were not able to be placed on the actual top or bottom face of the timber member. Instead, to collect a strain value at these locations, the strain gauge was placed on the side of the timber relatively close to the actual face of interest, i.e. the top or bottom face. However, the exact location on the side of these gauges was not

documented; hence it was difficult to theoretically estimate the strains at these locations. This difference in location of measurements between the field and analytical results may result in additional discrepancy between these values.

Also, the influence of the enlargement of the bolt hole or the release of the clamping forces that are used at each bolt to connect each of the individual members within the splice joint were not accounted for within the finite element models. This can be accomplished if the clamping force and the coefficient of friction between the individual members were known. In this case, an element can be used to model the sliding contact between the surfaces.

5.4.2 Member Dimensions

The dimensions of the timber members were assumed to be constant across the entire length when in actuality the dimensions varied across the entire length. Also, excluded within the dimensional properties of the timber is the presence of knots or imperfections along with checking within a timber member. These imperfections are difficult to categorize and quantify across the entire length of a specific timber let alone for each member within the bridge while also evaluating their influence on the structural performance of the timber member. Categorizing these findings within a finite element model for the historical timber bridges would require using solid elements in modeling each member of the structure so that one can include local imperfections and any other deterioration that may exist.

5.4.3 Material Properties

As per structural analysis theory, the effect of the material Young's modulus is significant in the determination of the structure's stiffness. Therefore, it is important to realize that within modeling the bridge structures as utilized herein, one must use the most representative material modulus for the timber specimen of the bridge. Unfortunately, such information was not available at the time of conducting this analysis.

With communication and guidance from the FPL (Rammer, 2011), the range of the modulus of elasticity was estimated to be between 0.6×10^6 psi and 1.8×10^6 psi. From studies completed by FPL, the value of the modulus of elasticity may vary plus or minus twenty-five percent. Thus with a distribution of two standard deviations, the modulus of elasticity value

could potentially fall within the above range. Hence, the deflection associated with this range of $0.6x10^6$ psi and $1.8x10^6$ psi for model VIII of the Zacke Cox Bridge will be 0.083 in. and 0.028 in., respectively.

Within the analytical models, each beam element was assumed to behave elastically thus not taking into account the non-linear behavior of the timber. Also, a homogenous material type was assumed within the analysis when in reality timber material is not a homogenous material and the timber members may have defects or weathering effects that cause uncertainty within this assumption. The orientation of the timber fiber with respect to the field strain measurement may not be perfectly parallel to each other, also causing a discrepancy between both the field and analytical results.

5.4.4 Truck Loading Distribution

When evaluating the percentage difference in the deflection that was caused by the small and large load truck in the Zacke Cox Bridge, one may notice that with the increased load, the percent difference between the measured and the calculated deflection increased from 20.95% to 58.24% for the small and large truck, respectively. Since the only change in the load idealization was the distribution quantity and location of the truck axles, one would have expected the change in the measured or calculated deflections to be proportioned to the applied loads. Furthermore, examining the field test results indicated that both main supporting elements, i.e., the two trusses, experienced different deflection (see Figure 5.13) even though the truck load was symmetrically applied on the bridge deck. These observations suggest that the load distribution is more complex than just dividing the applied loads equally between the two trusses. Through improved strain measurements and placement in the bridge structure could help in understanding how applied loads are distributed in these types of bridges.

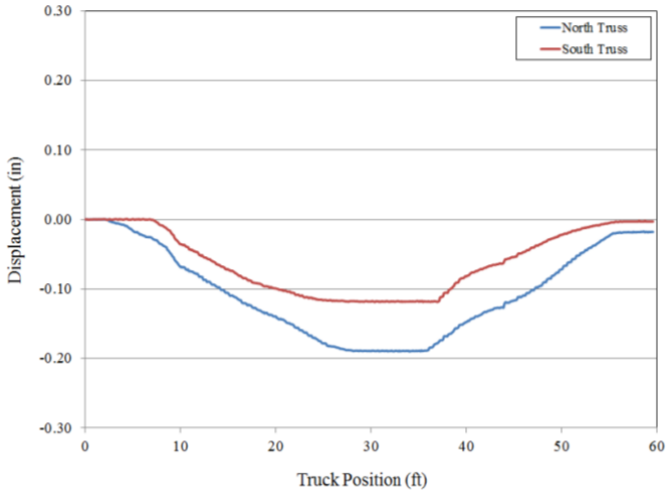

Figure 5.13: Deflection values for both the north and south truss as a function of the load truck position on the bridge (Zacke Cox Bridge) – large truck

5.4.5 Irregularities Present in the Bridges

Due to the length of time these bridges have been in service, there are characteristics that are both qualitative and quantitative which have not been introduced into the analytical models. With each bridge being uniquely different due to many events that the bridge has experienced such as construction methods, out of plane alignment of the truss and arch, deterioration due to time and weathering, and properties of the joints, just to name a few. Due to these irregularities, each bridge presents its own difficulties in accurately modeling a simplistic idealization. The following summarizes are some of the observations that were noticed in the field while testing the three bridges presented herein this study.

5.4.5.1 Zacke Cox Bridge

Even with the relatively short span of the Zacke Cox Bridge, there are a few irregularities that were not introduced into the analytical model. As can be seen in Figure 5.14.a, the arch of the truss is severely skewed out of plane with respect to the truss frame. In addition, it was noticed that there are pre-existing gaps between the vertical and diagonal members of the truss, as represented in Figure 5.14.b. Lastly, the Zacke Cox Bridge has a severe sag in the entire structure which can most evidently be seen in Figure 5.14.c. At mid-span, the permanent sag of the structure was measured to be approximately 3.5 in. None of these irregularities were introduced in the different analytical models of the bridge.

a. Arch out of plane

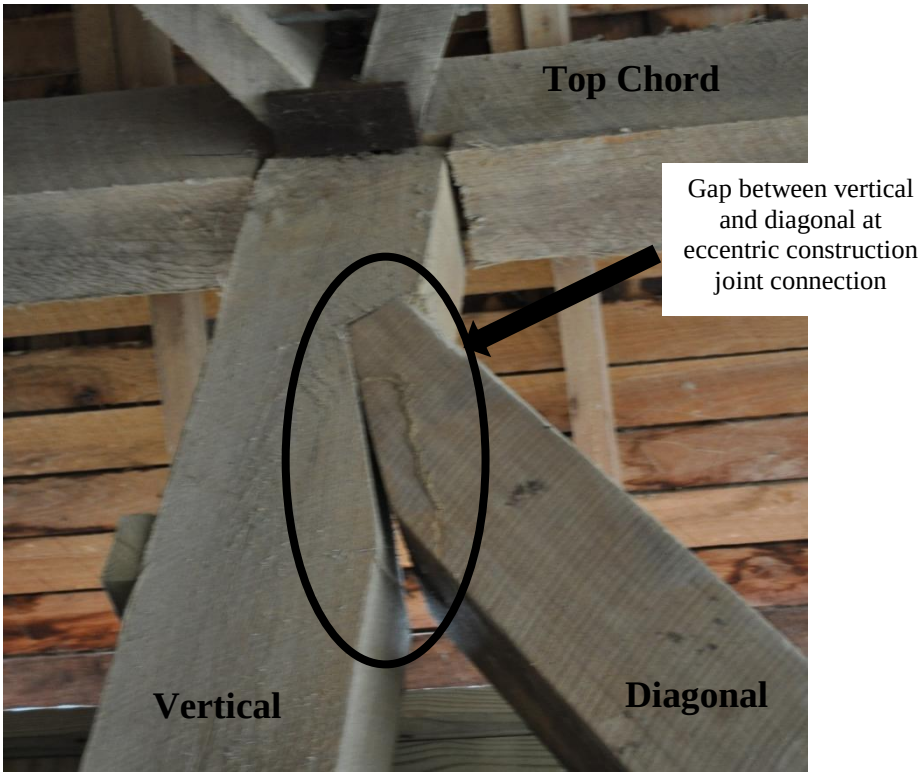

b. Gap between connections of timber members

c. Pre-existing sag in the overall bridge with measurement at mid-span

Figure 5.14: Irregularities present within the Zack Cox Bridge

5.4.5.2 Portland Mills Bridge

Just as in the Zacke Cox Bridge, there were pre-existing gaps between connection interfaces of the timber members. As can be seen in Figure 5.15.a, many vertical members within this bridge had a vertical misalignment with respect to the location of the connection between the top and bottom chord members. Furthermore, Figure 5.15.b shows some irregularities of how the ends of the arches were connected to the abutments. In addition, Figure 5.15.c shows deterioration to timber members such as the vertical member that could lead to a concern about the connection between those members, i.e. the vertical and bottom chord. These irregularities can easily affect the results of the analytical results but were not introduced into the analytical model.

a. Vertical skew of the vertical members

b. Alterations to the arch and abutment interaction

c. Connection of the vertical at the bottom chord

Figure 5.15: Irregularities present within the Portland Mills Bridge

5.4.5.3 Cox Ford Bridge

Many of the same irregularities such as the gap between the connections of timber members were also present within the Cox Ford Bridge. Just as in the other bridges, gaps between the splice joint and chord member existed. Many of these gaps are filled with gravel and debris which could alter the performance of the splice joint from its original intention. An example of the gaps between a bottom chord members and the splice joint is seen in Figure 5.16.a. Also, related to the concern of the splice joint performance, one bottom chord splice joint within the Cox Ford Bridge showed signs of failure between the connection of the chord member and joint material. Figure 5.16.b shows a portion of the bottom chord at the location of a splice joint that is detached from the rest of the bottom chord member. Within all the bridges, but especially in the Cox Ford Bridge, checking of the timber was present in many members. As can be seen in Figure 5.16.c, the length of the check and also depth into the member are a concern due to the effect on the load carrying capacity and dimensional properties of this member.

a. Gaps within the interface between the bottom chords and splice joint

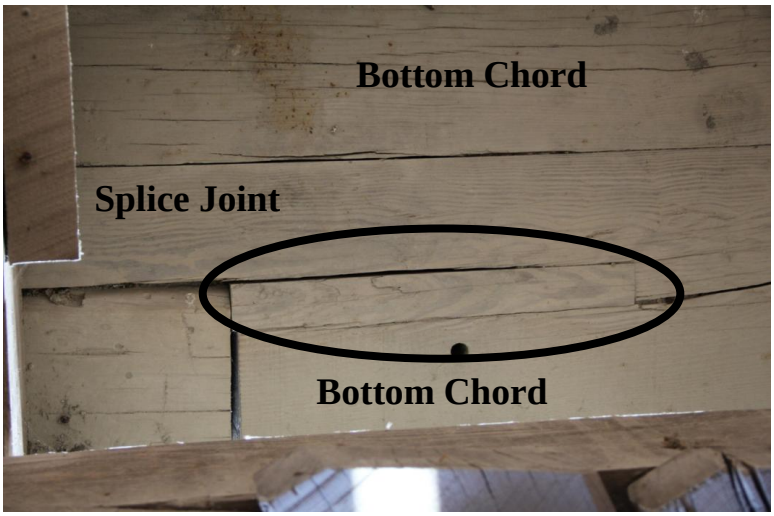

b. Failure between the bottom chord and splice joint

c. Length and depth of checks within timber members

Figure 5.16: Irregularities present within the Cox Ford Bridge

5.4.6 Influence of the Vertical Siding

The presence of the vertical side paneling on each bridge could easily have some effect on the overall structural behavior of the covered timber bridges. This effect was not explicitly examined in this study presented herein. Including the siding panel would require the knowledge of the dimensions, material properties and how these panels are connected to the main supporting elements. Including these elements in a model will increase the stiffness of the structure and hence reduce the overall deflection and induced strain values on the structural members under the vehicular loads.

CHAPTER 6: CONCLUSIONS

6.1 Summary

With the growing need to understand complex structures such as bridges for historical preservation, simple models that can be generalize to multiple circumstances but still take into account the as built considerations of a bridge are needed. This type of evaluation is needed to better assess the structure's behavior which in turn can lead to improved analytical techniques that better predict the load carrying capacity of the bridge. None of this could be more true than for the current historical timber covered bridges across the United States. Due to the number of different bridge types along with the construction method varying from bridge to bridge, these types of structures are difficult for a bridge engineer to evaluate accurately. Many times, there are inconsistencies with assumptions that are made by bridge engineers when analyzing such a complex structure like a Burr arch truss. With improved analytical modeling techniques, more appropriate and realistic rehabilitation efforts can be completed on these bridges along with improving bridge evaluation and rating calculations.

To accomplish the above objectives, both field testing and analytical models were developed for three Burr arch trusses located in Parke County, Indiana. During the field testing, displacement and strain values were collected at multiple locations. Analytical models were developed for each of the tested bridges utilizing the ANSYS finite element software. Construction details such as splice joints, boundary conditions and connection details between the different elements in the bridge structure were included within the models. The analytical models were evaluated and validated with respect to the field data results to determine the most appropriate modeling idealization for these specific types of bridges. From these findings and the evaluation, a recommendation of the most appropriate analytical models that can be used to assist bridge engineers in analyzing historical timber covered bridges.

6.2 Conclusion

From the discussions that were presented in this study, the following conclusions were attained:

- Finite element analysis is acceptable to investigate the behavior of Burr arch timber covered bridge.
    - The three dimensional finite element stick model showed that the arch contributed to the load carrying capacity of the bridge. For example, the analytical mid-span deflection for the truss-arch (model VIII) was 0.041 in. while for the truss only (model IX) was 0.076 in.
    - Even though there are discrepancies between the calculated strains, the finite element results show the correct direction of the strain in the truss and arch members.
    - The finite element and field measured deflections were comparable.
- A three dimensional finite element stick model idealization of one of the main supporting elements, i.e., the truss-arch elements, could be used to study the behavior of the truss-arch structure of a historical covered timber bridge. In this idealization, three dimensional beam elements could be utilized to represent the bridge timber members.
- The finite element model must take into consideration characteristics and geometry as presently seen within the structure.
- The finite element model must include the splice joints both in the bottom and top chord members, connection eccentricity, details between timber members and modeling of the members per the as built geometry, i.e., two separate bottom chord and arch members. However, the finite element idealization of this splice joint is highly dependent on the actual design and behavior of this connection. In other words, one needs to know the sliding, vertical and rotation stiffness of the splice joint.
- Idealizing the truss-arch structure excluding the eccentric in the connection between the vertical and diagonals, top chord and bottom chord members may yield a more stiff structure. For example, the finite element results showed

that the deflection calculations using model I was about 20% less than the calculated deflection of model VIII.

- Due to the relatively large influence on the overall bridge deflection and behavior, the species and modulus of elasticity for the timber is necessary to determine as accurately as possible.

The oversimplification of the covered timber bridge to include only one main supporting element implies that bridge engineers will also need to evaluate and determine the effect of other factors influences on the overall bridge behavior. These factors can influence the assumptions an engineer makes on how the applied loads are transferred to each of the two main supporting components.

6.3 Recommendation

Combined with findings of previous studies and the study presented herein, further laboratory examinations of the joint behavior are needed. This will help to more accurately model the splice joints and represent the global behavior of covered historical timber bridges. In addition, a better understanding of the load transfer through the splice joint is necessary through field and laboratory testing. This will assist in investigating the different behavior of the as built joints. Also, further study to determine the effect on the load transfer in these types of timber bridges is needed. Such investigation can be carried out using a three dimensional model of the entire bridge structure including the bridge deck, floor joists, floor beams, roof bracings, vertical sidings and the two main supporting structural components. This idealization is necessary to investigate the effects of these components on the overall rigidity of the structure within these types of bridges.

BIBLIOGRAPHY

ANSYS. 2011. User's manual for revision 12.1, Procedures. Canonsburg, PA: Swanson Analysis Systems, Inc.

Clark Dietz. Parke County Bridge No. 63 Special Feature Bridge Inspection. Indianapolis, IN: Clark Dietz, Inc. 2009. Print.

Clark Dietz. Parke County Bridge No. 155 Special Feature Bridge Inspection. Indianapolis, IN: Clark Dietz, Inc. 2009. Print.

Clark Dietz. Parke County Bridge No. 227 Special Feature Bridge Inspection. Indianapolis, IN: Clark Dietz, Inc. 2009. Print.

Forest Products Laboratory. Second Edition. Wood Engineering Handbook. Gen. Tech. Rep. Madison, WI: U. S. Department of Agriculture, Forest Service, Forest Products Laboratory. 4-13 p.

"History of Covered Bridges." *Welcome to the GDOT*. Georgia Department of Transportation. Web. 29 July 2010. <http://www.dot.state.ga.us/travelingingeorgia/bridges/coveredbridges/Pages/HistoryofCoveredBridges.aspx>.

Indiana Department of Transportation. Bridge Plans for Spans over 6.1 Meters Parke County 500 South (2) over Rock Run Creek. INDOT Project No. STP-9961. 2001. Print.

Indiana Department of Transportation. Bridge Plans for Spans over 20 Feet on 650 N. in Parke County Portland Mills Bridge. Project: MASTP-9961 (8) Const. 1995. Print.

Lamar, Dylan M., and Benjamin W. Schafer. 2004. "Structural Analyses of Two Historic Covered Wooden Bridges." Journal of Bridge Engineering. Nov./Dec. Vol. 9 Num. 6. 2004: 623-33. Print.

Loiselle, Kevin R. "Rehabilitation of Zacke Cox Bridge." E-mail interview. 16 May 2011.

Marston, Christopher H. Craftsmanship Across the Cornfields: A survey of Midwestern Covered Bridges. Washington, DC: National Park Service. 2006.

Parke County, IN. Covered Bridges. Zacke Cox Covered Bridge. 2011. <http://www.coveredbridges.com/index.php/covered_bridges?cfid=52>.

Parke County, IN. Covered Bridges. Zacke Cox Covered Bridge. 2011. <http://www.coveredbridges.com/index.php/poi_detail?poiID=10>.

Parke County, IN. Covered Bridges. Zacke Cox Covered Bridge. 2001. <http://www.coveredbridges.com/index.php/poi_detail?poiID=58>.

Rammer, Douglas. "Material properties." E-mail interview. 16 June 2011.

Sangree, Rachel H., and B. W. Schafer. "Experimental and numerical analysis of a halved and tabled traditional timber scarf joint". *Construction and Building Materials.* Feb. Vol. 23. Issue 2. 2009: 615-614. Print.

Sangree, Rachel H., and B. W. Schafer. "Experimental and numerical analysis of a stop-splayed traditional timber scarf joint with key". *Construction and Building Materials.* Jan. Vol. 23. Issue 1. 2009: 376-385. Print.

Sangree, Rachel H. 2006. *Covered Wooden Bridges: An Experimental and Numerical Investigation of System and Component Behavior.* Diss. Johns Hopkins University.

US Department of Transportation Federal Highway Administration. *Covered Bridge Manual.* Rep. no. FHWA-HRT-04-098. McLean, VA: Federal Highway Administration, 2005. Print.

APPENDIX

A.1 Cox Ford Bridge

A.1.1 Deflection Results at the Mid-Span and Quarter-Span Points

Figure A.1 shows the plots of the quarter and mid-span deflection results from the field testing as a function of the load truck position for both the small and large load truck. A downward deflection of 0.063 in. and 0.024 in. for the mid and quarter-spans, respectively, was recorded during the field testing within the east truss due utilizing the small truck. While for the large truck, within the field test results a downward deflection of 0.083 in. and 0.022 in. for the mid and quarter-spans were recorded, respectively. Tables A.1 and A.2 list the field results and analytical model deflection results both at mid and quarter-spans points.

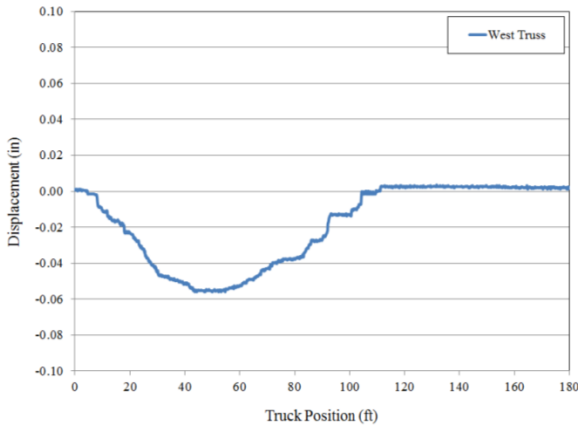

a. Quarter-span deflection –small truck

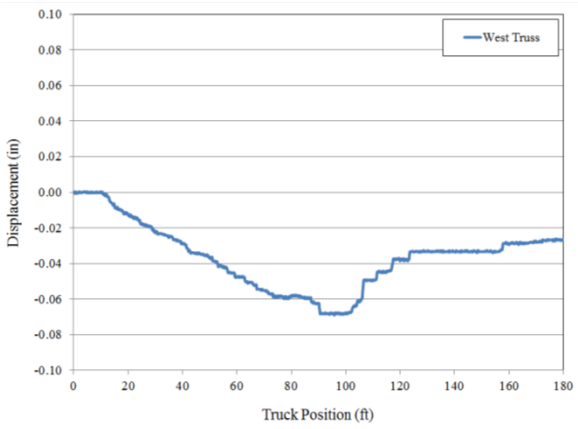

b. Mid-span deflection –small truck

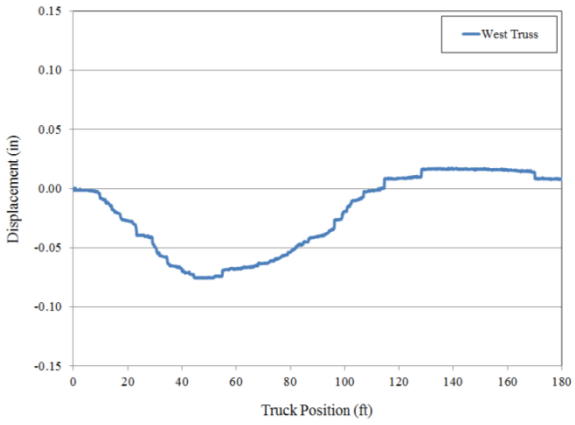

c. Quarter-span deflection – large truck

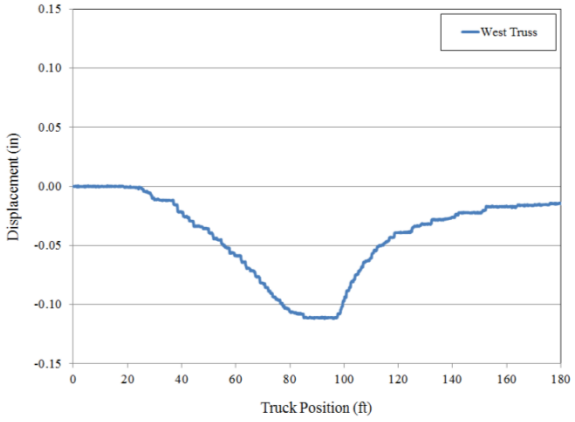

d. Mid-span deflection – large truck

Figure A.1: Small and large truck bridge deflection results for the Cox Ford Bridge as a function of the load truck position on the bridge (run down the centerline of the bridge)

Table A.1: Analytical deflection results for the Cox Ford Bridge – small truck

Model Number	Mid-span Deflection (in.)		Quarter-span Deflection (in.)	
	Analytical	Field	Analytical	Field
Cox Ford	0.166	0.063	0.071	0.024

Table A.2: Analytical deflection results for the Cox Ford Bridge – large truck

Model Number	Mid-span Deflection (in.)		Quarter-span Deflection (in.)	
	Analytical	Field	Analytical	Field
Cox Ford	0.288	0.083	0.120	0.022

Tables A.1 and A.2 suggest that a portion of the structure that influences the global deflection of the bridge was excluded within the analytical model. Thus without as built plan sheets and potential miss measurement of the timber dimensions and intersection points during the field testing could led to such discrepancies between the field and analytical results. Upon further information, the Cox Ford model will be reevaluated and modeled to represent those findings.

A.1.2 Deflection in the Vicinity of the Splice Joint

As can be seen in the deflected shapes below in Figures A.2 and A.3, many of the same conclusions as to the response and expected strain values can be made as was done within the Zacke Cox Bridge.

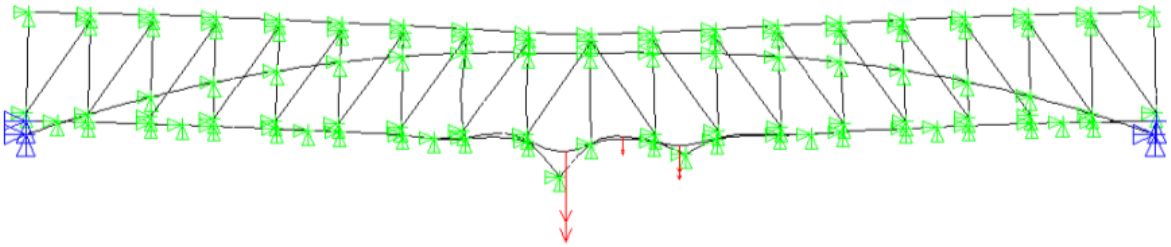

Figure A.2: Elevation view of the analytical deflected shape for the Cox Ford Bridge

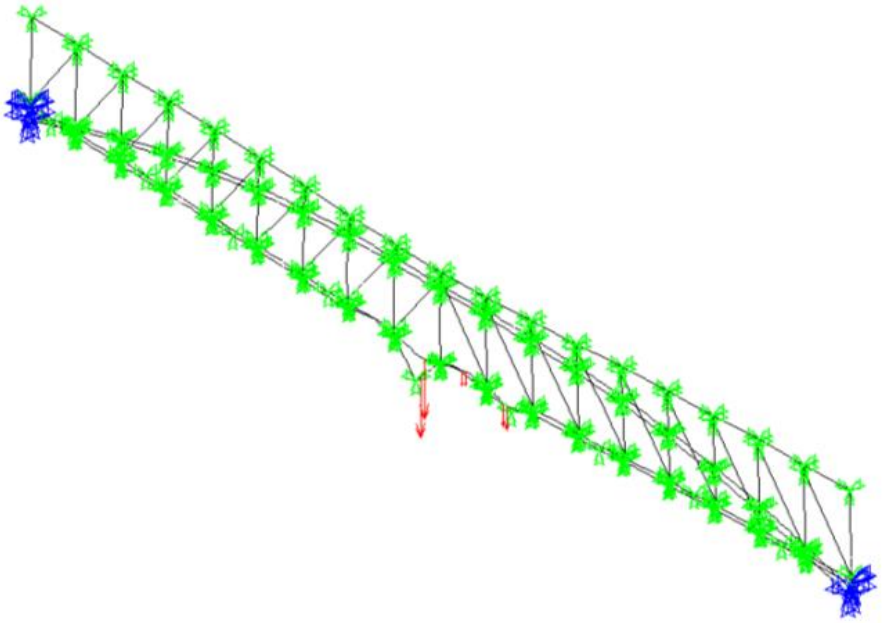

Figure A.3: Analytical deflected shape for the Cox Ford Bridge

A.1.3 Strain Results

Field recorded strain values were compared with the analytical strain values at each specific location within the truss that was evaluated. The locations of interest may be seen in Figure A.4. Table A.3 summarizes the field and analytical values. Due to the discrepancies between the field and analytical deflections results for both the small and large load truck tests, only the small truck strain values were compared for the fact that the difference between the field and analytical values was less than with the large truck.

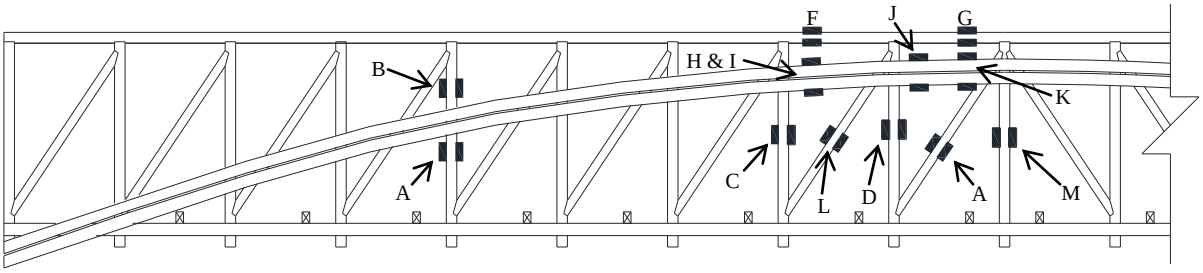

Figure A.4: Strain gauge truss locations for the Cox Ford Bridge - east truss south end between verticals 1 to 11

Table A.3: Field and analytical strain results for the Cox Ford Bridge - small truck

	Strain Gauge Location	Member Description	Field testing top (μ strain)	ANSYS top (μ strain)	Field testing bottom (μ strain)	ANSYS bottom (μ strain)
East Truss	A	Vertical 5	7	10	5	10
	B	Vertical 5	1	8	7	8
	C	Vertical 8	11	17	4	17
	D	Vertical 9	13	24	8	24
	E	Vertical 10	17	23	-10	23
	F**	Top chord – 8 and 9	-9	-28	-10	-28
	G**	Top chord – 9 and 10	-13	-37	-20	-37
	H	Arch – outward – 8 and 9	-1	-20	-7	-26
	I	Arch inward – 8 & 9	-4	-20	-23	-26
	J**	Arch outward – 9 and 10	0	-21	-23	-28
	K	Arch inward – 9 & 10	-4	-21	-22	-28
	L	Diagonal – 8 & 9	-4	-29	-21	-29
	M	Diagonal – 9 and 10	-11	-13	-17	-13

*Note: The top of the members is that of which is on the left when looking directly at the elevation view.
**Note: The top strain gauge was placed on the side face of the timber instead of the top face and the location on the side face was not documented.

Table A.3 shows that many of the timber members within the structure have the value (top and bottom) controlled by the axial strain due to a consistent value which is not validated with the field tests results.

Also, six strain gauges were placed on the bottom chord splice joint on the west and east trusses (i.e., three gauges on the top face and three gauges on the bottom face of the bottom chord splice joints). The locations of these specific strain gauges within the splice joint vicinity are seen in Figures A.5 and A.6. Table A.4 summarizes the values for both the field and analytical strain values and magnitudes.

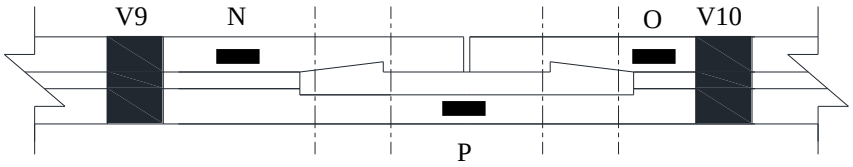

Figure A.5: Plan view of bottom chord joint with strain gauge locations on the west truss

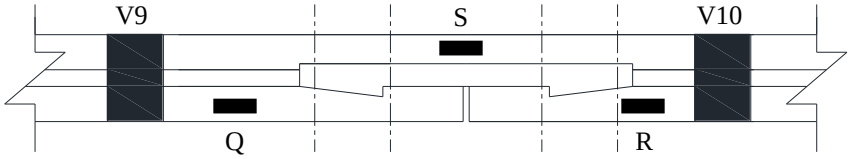

Figure A.6: Plan view of bottom chord joint with strain gauge locations on the east truss

Table A.4: Field and analytical strain results for splice joints for the Cox Ford Bridge – small truck

	Strain Gauge Location	Field testing top (μ strain)	ANSYS top (μ strain)	Field testing bottom (μ strain)	ANSYS bottom (μ strain)
West Truss	N	14	21	3	21
	O	22	21	-13	21
	P	31	21	-9	21
East Truss	Q	16	21	10	21
	R	14	21	-2	21
	S	30	21	-37	21

Just as in Table A.3, Table A.4 shows that the bottom chord members near the spliced joint vicinity have the value controlled by the axial strain due to the consistent value of the strain on both the top and bottom faces within the analytical model. The field test results do not validate this analytical finding. Thus, upon further details becoming available, this analytical model will be reevaluated.